

# Study of one-dimensional nature of $(\text{Sr,Ba})_2\text{Cu}(\text{PO}_4)_2$ and $\text{BaCuP}_2\text{O}_7$ via $^{31}\text{P}$ NMR.

R. Nath,<sup>1</sup> A. V. Mahajan,<sup>1</sup> N. Büttgen,<sup>2</sup> C. Kegler,<sup>2</sup> and A. Loidl<sup>2</sup>

<sup>1</sup>*Department of Physics, Indian Institute of Technology, Mumbai 400076, India*

<sup>2</sup>*Experimentalphysik V, Elektronische Korrelationen und Magnetismus,  
Institut für Physik, Universität Augsburg, D-86135 Augsburg, Germany.*

(Date textdate; Received textdate; Revised textdate; Accepted textdate; Published textdate)

## Abstract

The magnetic behavior of the low-dimensional phosphates  $(\text{Sr,Ba})_2\text{Cu}(\text{PO}_4)_2$  and  $\text{BaCuP}_2\text{O}_7$  was investigated by means of magnetic susceptibility and  $^{31}\text{P}$  nuclear magnetic resonance (NMR) measurements. We present here the NMR shift, the spin-lattice ( $1/T_1$ ) and spin-spin ( $1/T_2$ ) relaxation-rate data over a wide temperature range  $0.02 \text{ K} \leq T \leq 300 \text{ K}$ . The temperature dependence of the NMR shift  $K(T)$  is well described by the  $S = 1/2$  Heisenberg antiferromagnetic chain model (D.C. Johnston *et al.*, Phys. Rev. B **61**, 9558 (2000)) with an intrachain exchange of  $J/k_B \simeq 165 \text{ K}$ ,  $151 \text{ K}$ , and  $108 \text{ K}$  in  $\text{Sr}_2\text{Cu}(\text{PO}_4)_2$ ,  $\text{Ba}_2\text{Cu}(\text{PO}_4)_2$ , and  $\text{BaCuP}_2\text{O}_7$ , respectively. Deviations from Johnston's expression are seen for all these compounds in the  $T$ -dependence of  $K(T)$  at low temperatures.  $^{31}\text{P}$  is located symmetrically between the Cu ions and fluctuations of the staggered susceptibility at  $q = \frac{\pi}{a}$  should be filtered out due to vanishing of the geometrical form factor. However, the qualitative temperature dependence of our  $^{31}\text{P}$  NMR  $1/T_1$  indicates that relaxation due to fluctuations around  $q = \frac{\pi}{a}$  (but  $\neq \frac{\pi}{a}$ ) have the same  $T$ -dependence as those at  $q = \frac{\pi}{a}$  and apparently dominate. Our measurements suggest the presence of magnetic ordering at  $0.8 \text{ K}$  in  $\text{BaCuP}_2\text{O}_7$  ( $J/k_B \simeq 108 \text{ K}$ ) and a clear indication of a phase transition (divergence) in  $1/T_1(T)$ ,  $1/T_2(T)$ , and a change of the line shape is observed. This enables us to investigate the 1D behavior over a wide temperature range. We find that  $1/T_1$  is nearly  $T$ -independent at low-temperatures ( $1 \text{ K} \leq T \leq 10 \text{ K}$ ), which is theoretically expected for 1D chains when relaxation is dominated by fluctuations of the staggered susceptibility. At high temperatures,  $1/T_1$  varies nearly linearly with temperature, which accounts for contribution of the uniform susceptibility.

PACS numbers: 75.10.Pq, 75.40.Cx, 76.60.-k, 76.60.Cq

## I. INTRODUCTION

There is presently a lot of interest in the magnetic properties of one-dimensional (1D) Heisenberg antiferromagnetic (HAF) spin systems. This is due to the rich physics that they exhibit, in addition to the fact that such systems are tractable from a computational/theoretical standpoint. In particular, qualitative differences are expected between integer-spin and half-integer spin HAF chains. While the integer-spin chains are gapped,<sup>1</sup> the half-integer spin chains are said to have quasi long-range order (LRO) due to the gradual spatial decay (power-law) of the spin-spin correlation function.<sup>2,3</sup>

The magnetic Hamiltonian describing a spin-half Heisenberg chain can be written as  $H = -J \sum_i S_i \cdot S_{i+1}$  where  $J$  is the intrachain coupling constant between the nearest-neighbor spins. The temperature dependence of the magnetic susceptibility  $\chi(T)$  for the  $S = 1/2$  HAF chain was numerically calculated by Bonner and Fisher<sup>4</sup> and since then, the Bonner-Fisher expression has been used by experimentalists to determine the value of the exchange coupling ( $J$ ) from the temperature dependence of the bulk susceptibility. A more accurate and analytical evaluation of the susceptibility of  $S = 1/2$  HAF chain was done by Eggert, Affleck, and Takahashi<sup>5</sup> which is valid at low-temperatures. Via numerical simulations, an expression for  $\chi(T)$  accurate for both low and high temperatures ( $5 \times 10^{-25} \leq \frac{k_B T}{J} \leq 5$ , with  $k_B$  the Boltzmann constant) was given by Johnston *et al.*<sup>6</sup>. Dynamical properties of  $S = 1/2$  chains have also been theoretically investigated. In particular, work has been focussed on the properties measured by nuclear magnetic resonance (NMR) techniques. Sachdev<sup>7</sup> determined the temperature dependence of the NMR spin-lattice ( $1/T_1$ ) and the Gaussian spin-spin ( $1/T_{2G}$ ) relaxation rates for half-integer spin chains for  $\frac{k_B T}{J} \ll 1$  as:  $1/T_1 = \text{constant}$  and  $1/T_{2G} \propto 1/\sqrt{T}$ . Quantum Monte Carlo calculations by Sandvik<sup>8</sup> support these results over an appropriate temperature range. These results are at variance from those for classical spin chains ( $S = \infty$ ), where theory predicts<sup>9</sup>  $1/T_1$  and  $1/T_{2G} \propto T^{-3/2}$ .

While the 1D compounds  $\text{CuCl}_2 \cdot 2\text{NC}_5\text{H}_5$  and  $\text{KCuF}_3$  have been experimentally investigated previously,<sup>10,11</sup> the onset of LRO (at the ordering temperature  $T_N$ ) due to inter-chain interactions prevents the study of true 1D properties down to low temperatures. For the abovementioned 1D compounds, the ratios  $\frac{k_B T_N}{J} \simeq 0.084$  and  $0.1195$ , respectively, have been determined. Dynamic and static properties of  $\text{Sr}_2\text{CuO}_3$  1D chain have been extensively studied.<sup>12,13,14,15,16</sup> Due to the large value of  $J/k_B$  ( $\approx 2200$  K) and the very weak inter-chain

couplings, this compound orders only below 5 K and hence 1D properties could be studied in a large range of temperature. It is clearly useful to examine new compounds which might exhibit 1D behavior in a large temperature range, thereby allowing for a comparison with theoretical models and improving our understanding of such systems.

$\text{Sr}_2\text{Cu}(\text{PO}_4)_2$ <sup>17</sup> and  $\text{Ba}_2\text{Cu}(\text{PO}_4)_2$ <sup>18</sup> are two isostructural compounds having a monoclinic unit cell with space group  $C_{2/m}$ . The reported lattice constants are  $a = 11.515 \text{ \AA}$ ,  $b = 5.075 \text{ \AA}$ ,  $c = 6.574 \text{ \AA}$  and  $a = 12.160 \text{ \AA}$ ,  $b = 5.133 \text{ \AA}$ ,  $c = 6.885 \text{ \AA}$  for  $\text{Sr}_2\text{Cu}(\text{PO}_4)_2$  and  $\text{Ba}_2\text{Cu}(\text{PO}_4)_2$ , respectively.  $\text{BaCuP}_2\text{O}_7$ , which differs slightly in structure compared to the other two, crystallizes in a triclinic unit cell with space group  $P\bar{1}$  and lattice constants  $a = 7.353 \text{ \AA}$ ,  $b = 7.578 \text{ \AA}$ ,  $c = 5.231 \text{ \AA}$ .<sup>19</sup> In the former two compounds, each  $\text{CuO}_4$  square plane shares its edges with two similar kind of  $\text{PO}_4$  groups. The edge sharing takes place in one direction forming an isolated  $[\text{Cu}(\text{PO}_4)_2]_\infty$  chain along the crystallographic  $b$ -direction. A likely interaction path of  $\text{Cu}^{2+}$  ions is sketched in Fig. 1(a). As opposed to  $\text{Sr}_2\text{Cu}(\text{PO}_4)_2$  and  $\text{Ba}_2\text{Cu}(\text{PO}_4)_2$ ,  $\text{BaCuP}_2\text{O}_7$  contains two inequivalent P atoms, where each  $\text{CuO}_4$  plaquette shares its edges with two different  $\text{PO}_4$  groups forming chains as shown in Fig. 1(b). Unlike the isolated chains of  $\text{Sr}_2\text{Cu}(\text{PO}_4)_2$  and  $\text{Ba}_2\text{Cu}(\text{PO}_4)_2$ , there appear to be pairs of chains in  $\text{BaCuP}_2\text{O}_7$ . Detailed magnetic properties of these compounds have not been reported yet. Only Etheredge and Hwu<sup>18</sup> have published the bulk susceptibility as a function of temperature for  $\text{Ba}_2\text{Cu}(\text{PO}_4)_2$ . However, the authors failed to comment on the broad maximum at 80 K presumably because it was suppressed by a high Curie contribution present in their sample.

In this paper we present in detail the magnetic properties of the 1D copper phosphates,  $\text{Sr}_2\text{Cu}(\text{PO}_4)_2$ ,  $\text{Ba}_2\text{Cu}(\text{PO}_4)_2$ , and  $\text{BaCuP}_2\text{O}_7$  using  $^{31}\text{P}$  NMR as a local probe. NMR is regarded as a valuable tool for the study of microscopic properties of 1D chains, especially through the studies of the NMR shift ( $K$ ), the spin-spin relaxation rate ( $1/T_2$ ), and the spin-lattice relaxation rate ( $1/T_1$ ). We report on measurements of the bulk susceptibility  $\chi(T)$  for  $1.8 \text{ K} \leq T \leq 400 \text{ K}$  and  $K(T)$ ,  $1/T_1(T)$ , and  $1/T_2(T)$  of  $^{31}\text{P}$  NMR in a large temperature range ( $0.02 \text{ K} \leq T \leq 300 \text{ K}$ ). The experimental details concerning sample preparation and various measurements are given in the next section. Section III contains our experimental results and a detailed discussion about the results is presented in section IV. Our work on these compounds strongly suggests that they are some of the best examples of  $S = 1/2$  1D HAF systems. In the course of our work, magnetic susceptibility and heat capacity of

$\text{Sr}_2\text{Cu}(\text{PO}_4)_2$ ,  $\text{Ba}_2\text{Cu}(\text{PO}_4)_2$ , and  $\text{BaCuP}_2\text{O}_7$  were reported by Belik *et al.*<sup>20,21</sup>. They found the exchange constant ( $J/k_B$ ) to be 144 K for  $\text{Sr}_2\text{Cu}(\text{PO}_4)_2$ , 132 K for  $\text{Ba}_2\text{Cu}(\text{PO}_4)_2$ , and 103.6 K for  $\text{BaCuP}_2\text{O}_7$ . Presence of any LRO was not seen from specific heat measurement down to 0.45 K for  $\text{Sr}_2\text{Cu}(\text{PO}_4)_2$  and  $\text{Ba}_2\text{Cu}(\text{PO}_4)_2$ , whereas  $\text{BaCuP}_2\text{O}_7$  showed ordering at 0.81 K.

## II. EXPERIMENTAL DETAILS

Polycrystalline samples of  $\text{Sr}_2\text{Cu}(\text{PO}_4)_2$ ,  $\text{Ba}_2\text{Cu}(\text{PO}_4)_2$ , and  $\text{BaCuP}_2\text{O}_7$  were prepared by solid state reaction techniques using  $\text{BaCO}_3$  (99.9% pure),  $\text{SrCO}_3$  (99.999% pure),  $\text{CuO}$  (99.99% pure) and  $(\text{NH}_4)_2\text{HPO}_4$  (99.9% pure) as starting materials. The stoichiometric mixtures were fired at 800 °C ( $\text{Sr}_2\text{Cu}(\text{PO}_4)_2$ ), 700 °C ( $\text{Ba}_2\text{Cu}(\text{PO}_4)_2$ ) and 650 °C ( $\text{BaCuP}_2\text{O}_7$ ) for 120 hours each, in air, with several intermediate grindings and pelletization. Finally some amounts of each of the samples were annealed at 400 °C under a reducing atmosphere (5%  $\text{H}_2$  in Ar) in an attempt to reduce the Curie contribution in the bulk susceptibility. Nearly single phases were confirmed from x-ray diffraction, which was performed with a Philips Xpert-Pro powder diffractometer. A Cu target was used in the diffractometer with  $\lambda_{av} = 1.54182$  Å. The x-ray diffraction patterns are shown in Fig. 2. Only one compound ( $\text{Sr}_2\text{Cu}(\text{PO}_4)_2$ ) exhibits minor impurity peaks which are marked by asterisks. Lattice parameters were calculated using a least-square fit procedure. The obtained lattice constants are ( $a = 11.496(5)$  Å,  $b = 5.069(2)$  Å,  $c = 6.566(3)$  Å), ( $a = 12.138(2)$  Å,  $b = 5.123(1)$  Å,  $c = 6.868(1)$  Å) and ( $a = 7.338(2)$  Å,  $b = 7.561(2)$  Å,  $c = 5.217(1)$  Å) for  $\text{Sr}_2\text{Cu}(\text{PO}_4)_2$ ,  $\text{Ba}_2\text{Cu}(\text{PO}_4)_2$ , and  $\text{BaCuP}_2\text{O}_7$ , respectively. These are in agreement with previously reported values.

Magnetization ( $M$ ) data were measured as a function of temperature  $T$  ( $1.8 \text{ K} \leq T \leq 400 \text{ K}$ ) and applied field  $H$  ( $0 \leq H \leq 70 \text{ kG}$ ) using a SQUID magnetometer.

The NMR measurements were carried out using pulsed NMR techniques on  $^{31}\text{P}$  nuclei (nuclear spin  $I = 1/2$  and gyromagnetic ratio  $\gamma/2\pi = 17.237 \text{ MHz/Tesla}$ ) in a large temperature range ( $0.02 \text{ K} \leq T \leq 300 \text{ K}$ ). We have done the measurements at two different applied fields of about 55 kG and 4 kG which correspond to radio frequencies (rf) of about 95 MHz and 6.8 MHz, respectively.

For  $2 \text{ K} \leq T \leq 300 \text{ K}$ , NMR measurements were done in a 55 kG applied field with a

$^4\text{He}$  cryostat (Oxford Instruments). Spectra were obtained by Fourier transform (FT) of the NMR echo signals using a  $\pi/2$  pulse of width of about  $4\ \mu\text{s}$ . The NMR shift  $K(T) = [\nu(T) - \nu_{ref}]/\nu_{ref}$  was determined by measuring the resonance frequency of the sample ( $\nu(T)$ ) with respect to a standard  $\text{H}_3\text{PO}_4$  solution (resonance frequency  $\nu_{ref}$ ). The spin-lattice relaxation rate ( $1/T_1$ ) was determined by the inversion-recovery method. Spin-spin relaxation rate ( $1/T_2$ ) was obtained by measuring the decay of the echo integral with variable spacing between the  $\pi/2$  and the  $\pi$  pulse.

In the  $0.02\ \text{K} \leq T \leq 10\ \text{K}$  range, NMR measurements were performed using a  $^3\text{He}/^4\text{He}$  dilution refrigerator (Oxford Instruments) with the resonant circuit inside the mixing chamber. Spectra were obtained by field sweeps at a constant radio frequency ( $\nu_{rf}$ ) of 95 MHz.  $1/T_1$  was measured down to 0.02 K following the same procedure as described above using  $\pi/2$  pulse of width  $15\ \mu\text{s}$ . Lower rf power (and consequently longer pulse widths) were used to avoid rf heating of the sample. Measurements were also done in a low-field of about 4 kG ( $\nu_{rf} \simeq 6.8\ \text{MHz}$ ) where the NMR line was narrow and inversion of the nuclear magnetization by a  $\pi$  pulse of width  $30\ \mu\text{s}$  was assured. The data from low-field measurements almost reproduce the high-field data.

### III. RESULTS

#### A. Bulk Susceptibility

Magnetic susceptibilities  $\chi(T)$  ( $= M/H$ ) for all the three compounds were measured as a function of temperature in an applied field of 5 kG (Fig. 3). The amount of ferromagnetic impurities present in our samples were estimated from the intercept of  $M$  vs.  $H$  isotherms at various temperatures and were found to be 19 ppm, 12 ppm, and 30 ppm of ferromagnetic  $\text{Fe}^{3+}$  ions for  $\text{Sr}_2\text{Cu}(\text{PO}_4)_2$ ,  $\text{Ba}_2\text{Cu}(\text{PO}_4)_2$ , and  $\text{BaCuP}_2\text{O}_7$ , respectively. The data in Fig. 3 have been corrected for these ferromagnetic impurities. As shown in the figure, all the samples exhibit a broad maximum, indicative of low-dimensional magnetic interactions. With decrease in temperature, susceptibility increases in a Curie-Weiss manner. This possibly comes from chain ends, natural defects, excess oxygen and extrinsic paramagnetic impurities present in the samples. No obvious features associated with LRO are seen for  $1.8\ \text{K} \leq T \leq 400\ \text{K}$  for any of the samples. A substantial reduction of Curie terms was achieved by

annealing the samples at 400 °C in an atmosphere of 5% H<sub>2</sub> in Ar. Similar experiments in Sr<sub>2</sub>CuO<sub>3</sub> and Y<sub>2</sub>BaNiO<sub>5</sub> lead to reduced Curie terms.<sup>22,23</sup> In the insets of Figs. 3(a) and 3(b), data for as-prepared and reduced Sr<sub>2</sub>Cu(PO<sub>4</sub>)<sub>2</sub> and Ba<sub>2</sub>Cu(PO<sub>4</sub>)<sub>2</sub>, respectively are shown. Since the Curie contribution in the case of as-prepared BaCuP<sub>2</sub>O<sub>7</sub> is not large, we did not treat this sample in a reducing atmosphere.

In order to fit the bulk susceptibility data, we assume that the susceptibility consists of three terms:

$$\chi = \chi_0 + \frac{C}{T + \theta} + \chi_{spin}(T) \quad (1)$$

where  $\chi_{spin}(T)$  is the uniform spin susceptibility for a  $S = 1/2$  1D HAF system given in Ref. 6 (expression corresponding to “fit2”). This expression (containing the the Landé  $g$ -factor and  $J$  as fitting parameters) is not reproduced here since it is somewhat unwieldy. The first term  $\chi_o$  is temperature independent and consists of diamagnetism of the core electron shells ( $\chi_{core}$ ) and Van-Vleck paramagnetism ( $\chi_{vv}$ ) of the open shells of the Cu<sup>2+</sup> ions present in the sample. The second term  $\frac{C}{T+\theta}$  is the Curie-Weiss contribution due to paramagnetic species in the sample.

The average Landé  $g$ -factors determined from an analysis of the powder spectra from electron paramagnetic resonance (EPR) experiments on our samples were found to be 2.15, 2.15, and 2.2 for Sr<sub>2</sub>Cu(PO<sub>4</sub>)<sub>2</sub>, Ba<sub>2</sub>Cu(PO<sub>4</sub>)<sub>2</sub>, and BaCuP<sub>2</sub>O<sub>7</sub>, respectively. Our experimental  $\chi(T)$  data were fitted using the above  $g$ -values (the solid lines are the best fits in Fig. 3) and the extracted parameters are listed in Table I.

Table I.

| Sample  | $\chi_0$                               | $C$                                     | $\theta$ | $\frac{J}{k_B}$ |
|---|--|---|----------|-----------------|
|   | 10 <sup>-3</sup> cm <sup>3</sup> /mole | 10 <sup>-3</sup> cm <sup>3</sup> K/mole | K        | K               |
| Sr <sub>2</sub> Cu(PO <sub>4</sub> ) <sub>2</sub> | 0.005                                  | 10.6                                    | 1.1      | 152             |
| Ba <sub>2</sub> Cu(PO <sub>4</sub> ) <sub>2</sub> | -0.15                                  | 6.8                                     | 0.5      | 146             |
| BaCuP <sub>2</sub> O <sub>7</sub>                 | -0.07                                  | 1.6                                     | 0.4      | 108             |

Adding the core diamagnetic susceptibility for the individual ions<sup>24</sup>, the total  $\chi_{core}$  was calculated to be  $-1.39 \times 10^{-4}$  cm<sup>3</sup>/mole,  $-1.73 \times 10^{-4}$  cm<sup>3</sup>/mole, and  $-1.29 \times 10^{-4}$  cm<sup>3</sup>/mole for Sr<sub>2</sub>Cu(PO<sub>4</sub>)<sub>2</sub>, Ba<sub>2</sub>Cu(PO<sub>4</sub>)<sub>2</sub>, and BaCuP<sub>2</sub>O<sub>7</sub>, respectively. The Van-Vleck paramagnetic

susceptibility for our samples estimated by subtracting  $\chi_{core}$  from  $\chi_0$  gives  $\chi_{vv} = 14.4 \times 10^{-5}$  cm<sup>3</sup>/mole,  $2.3 \times 10^{-5}$  cm<sup>3</sup>/mole, and  $5.9 \times 10^{-5}$  cm<sup>3</sup>/mole for Sr<sub>2</sub>Cu(PO<sub>4</sub>)<sub>2</sub>, Ba<sub>2</sub>Cu(PO<sub>4</sub>)<sub>2</sub>, and BaCuP<sub>2</sub>O<sub>7</sub>, respectively. These values are comparable to that found in Sr<sub>2</sub>CuO<sub>3</sub><sup>12</sup>. The Curie contributions present in the samples correspond to a defect spin concentration of 3 %, 1.8 % and 0.4 % for Sr<sub>2</sub>Cu(PO<sub>4</sub>)<sub>2</sub>, Ba<sub>2</sub>Cu(PO<sub>4</sub>)<sub>2</sub>, and BaCuP<sub>2</sub>O<sub>7</sub>, respectively assuming defect spin  $S = 1/2$ .

## B. <sup>31</sup>P NMR

### 1. NMR shift

NMR has an important advantage over bulk susceptibility for the determination of magnetic parameters. While the presence of a Curie-like contribution restricts the accurate determination of  $\chi_{Spin}(T)$  and hence  $J$  from  $\chi(T)$ , in NMR this paramagnetism broadens the NMR line but does not contribute to the NMR shift  $K$ . Therefore, it is more reliable to extract the  $\chi_{Spin}(T)$  and  $J$  from the temperature dependence of the NMR shift rather than from the bulk susceptibility. From Fig.1 it appears that in all the compounds each <sup>31</sup>P is coupled to two Cu<sup>2+</sup> ions via a super-transferred hyperfine interaction mediated by oxygen ions in its neighborhood. All the NMR data reported in this paper correspond to samples of Sr<sub>2</sub>Cu(PO<sub>4</sub>)<sub>2</sub> and Ba<sub>2</sub>Cu(PO<sub>4</sub>)<sub>2</sub> which were treated in a reducing atmosphere as described in the previous section while the data for BaCuP<sub>2</sub>O<sub>7</sub> correspond to the as-prepared sample. We note here that we also did NMR measurements on the as-prepared Sr<sub>2</sub>Cu(PO<sub>4</sub>)<sub>2</sub> and Ba<sub>2</sub>Cu(PO<sub>4</sub>)<sub>2</sub> samples (for  $T > 10$  K) and found no differences with respect to the samples which were treated in a reducing atmosphere.

NMR shift data as a function of temperature are shown in Fig. 4. The samples exhibit broad maxima at different temperatures:  $\approx 100$  K for Sr<sub>2</sub>Cu(PO<sub>4</sub>)<sub>2</sub>,  $\approx 90$  K for Ba<sub>2</sub>Cu(PO<sub>4</sub>)<sub>2</sub>, and  $\approx 70$  K for BaCuP<sub>2</sub>O<sub>7</sub>, indicative of short-range ordering. Towards lower temperatures  $T < 20$  K, the NMR shift  $K(T)$  shows a plateau as is demonstrated by the semilogarithmic plot in the inset of Fig. 4. In the sub-Kelvin region, the NMR shift  $K(T)$  of all our samples decreases steeply. The fall-off appears below  $k_B T/J \simeq 0.003$  for Sr<sub>2</sub>Cu(PO<sub>4</sub>)<sub>2</sub>,  $k_B T/J \simeq 0.0033$  for Ba<sub>2</sub>Cu(PO<sub>4</sub>)<sub>2</sub>, and  $k_B T/J \simeq 0.01$  for BaCuP<sub>2</sub>O<sub>7</sub>.

The conventional scheme of analysis is to first determine the spin susceptibility (as done

in the previous section) and then plot  $K$  vs  $\chi_{spin}$  with  $T$  as an implicit parameter. The exchange coupling  $J$  is obtained from the susceptibility analysis while the slope of the  $K$  vs  $\chi_{spin}$  plot yields the total hyperfine coupling  $A$  between the  $^{31}\text{P}$  nucleus and the two nearest-neighbor  $\text{Cu}^{2+}$  ions. As an example, such a  $K - \chi_{spin}$  plot is shown in Fig. 5 for  $\text{BaCuP}_2\text{O}_7$ .

Since an algebraic expression for the temperature dependence of the spin susceptibility (and therefore the spin-shift) is known in this case, we prefer to determine  $J$  and  $A$  simultaneously by fitting the temperature dependence of  $K$  to the following equation,

$$K = K_0 + \left( \frac{A}{N_A \mu_B} \right) \chi_{spin}(T, J) \quad (2)$$

where  $K_0$  is the chemical shift and  $N_A$  is the Avogadro number. While fitting,  $g$  was kept fixed to the value obtained from EPR analysis and  $K_0$ ,  $A$ , and  $J$  were free parameters. The parameters  $J$  and  $A$  determined in this manner are considered more reliable, since the only temperature dependent term in the NMR shift is due to spin-susceptibility, while bulk susceptibility analysis is somewhat hampered by low-temperature Curie terms. As shown in Fig. 4, the shift data fit nicely to Eq. 2 in the temperature range  $10 \text{ K} \leq T \leq 300 \text{ K}$  yielding the parameters given in Table II.

Table II.

| Sample                                | $K_0$ | $A$            | $J/k_B$ |
|---------------------------------------|-------|----------------|---------|
|                                       | ppm   | Oe/ $\mu_B$    | K       |
| $\text{Sr}_2\text{Cu}(\text{PO}_4)_2$ | 47    | $2609 \pm 100$ | 165     |
| $\text{Ba}_2\text{Cu}(\text{PO}_4)_2$ | 40    | $3364 \pm 130$ | 151     |
| $\text{BaCuP}_2\text{O}_7$            | 73    | $2182 \pm 20$  | 108     |

## 2. Spectra

For all the three compounds the  $^{31}\text{P}$  NMR spectra consist of a single spectral line as is expected for  $I = 1/2$  nuclei (Fig. 6). As shown in the crystal structures in Fig. 1,  $\text{Sr}_2\text{Cu}(\text{PO}_4)_2$  and  $\text{Ba}_2\text{Cu}(\text{PO}_4)_2$  have a unique  $^{31}\text{P}$  site, whereas in  $\text{BaCuP}_2\text{O}_7$  there are two inequivalent  $^{31}\text{P}$  sites. However, a single resonance line even for  $\text{BaCuP}_2\text{O}_7$  implies that both the  $^{31}\text{P}$  sites in this compound are nearly identical. Since our measurements are



on randomly oriented polycrystalline samples, asymmetric shape of the spectra corresponds to a powder pattern due to an asymmetric hyperfine coupling constant and an anisotropic susceptibility. The linewidth was found to be field and temperature dependent as is shown in the insets of Figs. 6(a) and (b) for  $(\text{Sr/Ba})_2\text{Cu}(\text{PO}_4)_2$  and in Figs. 6(c) and (d) for  $\text{BaCuP}_2\text{O}_7$ , respectively. While we did not do a detailed analysis of the linewidth, its  $T$ - and  $H$ -dependence is likely due to macroscopic field inhomogeneities due to the demagnetization effects of a powder sample<sup>25</sup> and paramagnetic impurities.

As seen from Fig. 6 (c) the NMR spectra of  $\text{BaCuP}_2\text{O}_7$  broaden abruptly below about 0.8 K. We then measured the spectral lineshape in a low field ( $H \simeq 4$  kG) below 0.8 K in order to check whether any features could be resolved. Fig. 6 (d) shows the appearance of two shoulders on either side of the central line below 0.8 K. This is most likely an indication of the appearance of LRO. The positions of the shoulders stay unchanged with temperature while their relative intensity increases with decreasing temperature. A more detailed discussion is carried out in section IV.

### 3. Spin-lattice relaxation rate $1/T_1$

Temperature dependencies of  $^{31}\text{P}$   $1/T_1$  are presented in Fig.7. For the  $1/T_1$  experiment, the central positions of corresponding spectra at high (55 kG) and low (4 kG) external fields have been irradiated. Inset of Fig.7 (a) shows the typical magnetization recovery at  $H \simeq 55$  kG and at two different temperatures. For a spin-1/2 nucleus the recovery is expected to follow a single exponential behavior. In  $\text{Sr}_2\text{Cu}(\text{PO}_4)_2$  and  $\text{Ba}_2\text{Cu}(\text{PO}_4)_2$  (for  $H \simeq 55$  kG), the recovery of the nuclear magnetization after an inverting pulse was single exponential down to 2 K while for  $T < 2$  K, it fitted well to the double exponential,

$$\frac{1}{2} \left( \frac{M(\infty) - M(t)}{M(\infty)} \right) = A_1 \exp \left( -\frac{t}{T_{1L}} \right) + A_2 \exp \left( -\frac{t}{T_{1S}} \right) + C \quad (3)$$

where  $1/T_{1L}$  corresponds to the slower rate and  $1/T_{1S}$  is the faster component.  $M(t)$  is the nuclear magnetization a time  $t$  after an inverting pulse. Since the deviation from single exponential behavior could be due to the large linewidth and our consequent inability to saturate the NMR line, we also performed experiments at a lower field ( $\simeq 4$  kG), where the line is about three times narrower (see insets of Figs. 6 (a) or (b)). However, even in low-field (where the rf field  $H_1$  was sufficient to ensure complete inversion) the nuclear magnetization

recovery is not single exponential implying that this is an intrinsic effect. With increasing temperature, the ratio  $\frac{A_2}{A_1}$  decreases and the recovery becomes single exponential for  $T > 2$  K. It appears that the longer  $T_1$  component comes from the chain itself while the faster component is associated with  $^{31}\text{P}$  nuclei near chain ends. Clearly, at lower temperatures, the chain-end-induced magnetization extends to large distances from chain ends (thereby affecting more  $^{31}\text{P}$  nuclei) and consequently the weight associated with the faster relaxation is more at lower temperatures. From the experiment, it was found that low-field measurements reproduce almost the same  $T_1$  as for high-field.<sup>26</sup> Although we have measured  $T_1$  down to 0.02 K, since the magnetization recovery is not single-exponential, reliable relaxation rates  $1/T_1$  couldn't be obtained below 0.1 K (where the faster component  $1/T_{1s}$  has a large weight). Fig. 7 (a) and (b) display data down to 0.1 K, where it is seen that  $1/T_1$  for  $\text{Sr}_2\text{Cu}(\text{PO}_4)_2$  and  $\text{Ba}_2\text{Cu}(\text{PO}_4)_2$  do not show any anomaly. Even at lower temperatures, there was no indication of a divergence of the relaxation rate, indicating the absence of any magnetic ordering. For  $1 \text{ K} \leq T \leq 10 \text{ K}$ ,  $1/T_1$  remains constant with temperature and below 0.5 K a slight increase was observed for both  $\text{Sr}_2\text{Cu}(\text{PO}_4)_2$  and  $\text{Ba}_2\text{Cu}(\text{PO}_4)_2$ . At high temperatures ( $T \geq 30 \text{ K}$ ),  $1/T_1$  varies nearly linearly with temperature.

In  $\text{BaCuP}_2\text{O}_7$ ,  $1/T_1$  at  $H \simeq 55 \text{ kG}$  was measured down to 3 K. Once again, the large line width prevented us from saturating the nuclear magnetization below 3 K. Low-field measurements give perfect single exponential recovery down to 2 K and below 2 K, it was fitted well to double exponential. From Fig. 7(c), it is clear that the  $1/T_1(T)$  diverges at  $T \approx 0.8 \text{ K}$ , indicating an approach to magnetic ordering. For  $1 \text{ K} \leq T \leq 10 \text{ K}$ ,  $1/T_1$  remains constant and for  $T \geq 15 \text{ K}$ , it varies linearly with temperature. Slight change in magnitude in low-field data compared to high-field data may be due to spin-diffusion.<sup>13</sup>

#### 4. Spin-spin relaxation rate $1/T_{2G}$

Spin-spin relaxation was measured at  $H \simeq 4 \text{ kG}$ , where the line is sufficiently narrow. The spin-spin relaxation was found to have a Gaussian behavior and the rate ( $1/T_{2G}$ ) was obtained by monitoring the decay of the transverse magnetization after a  $\frac{\pi}{2} - t - \pi$  pulse sequence, as a function of the pulse separation time  $t$ , and fitting to the following equation,

$$M(2t) = M_0 \exp\left[-2\left(\frac{t}{T_{2G}}\right)^2\right] + C \quad (4)$$

As shown in the inset of Fig.8, the spin-spin relaxation rate  $1/T_{2G}$  for all the samples is nearly temperature independent.  $\text{BaCuP}_2\text{O}_7$  is the only compound which exhibits a significantly enhanced spin-spin relaxation rate  $1/T_{2G}$  at the lowest temperature compared to elevated temperatures. This increase of  $1/T_{2G}$  in  $\text{BaCuP}_2\text{O}_7$  is most likely related to LRO.

## IV. DISCUSSION

### A. NMR shift

The general variation of the shift with temperature follows the expected behavior of an  $S = 1/2$  HAF chain, as seen in the results section. A steep decrease in  $K(T)$  was observed below  $k_B T/J \simeq 0.003$  for  $\text{Sr}_2\text{Cu}(\text{PO}_4)_2$ ,  $k_B T/J \simeq 0.0033$  for  $\text{Ba}_2\text{Cu}(\text{PO}_4)_2$  and  $k_B T/J \simeq 0.01$  for  $\text{BaCuP}_2\text{O}_7$ .<sup>27</sup> This decrease of  $K$  is clearly much more than the logarithmic decrease with an infinite slope at zero temperature, expected from theory (see solid line in Fig. 4). In  $\text{Sr}_2\text{Cu}(\text{PO}_4)_2$ ,  $\text{Ba}_2\text{Cu}(\text{PO}_4)_2$ , and  $\text{BaCuP}_2\text{O}_7$ , from Fig. 4, the extrapolated shifts at zero temperature were found to be 400 ppm, 590 ppm, and 580 ppm, respectively. The theoretically expected values, derived from the  $T = 0$  susceptibility<sup>28</sup> and using the relevant  $A$  and  $K_0$ , are 544 ppm, 740 ppm, and 738 ppm, respectively for  $\text{Sr}_2\text{Cu}(\text{PO}_4)_2$ ,  $\text{Ba}_2\text{Cu}(\text{PO}_4)_2$ , and  $\text{BaCuP}_2\text{O}_7$ . Among the various causes for this deviation, one might be the onset of spin-Peierls order. In such a case, the spin susceptibility (and therefore the spin shift) should vanish at  $T = 0$ . However, our extrapolated  $T = 0$  shifts are much more than the chemical shifts  $K_0$  and there is no exponential decrease of  $1/T_1(T)$  toward low temperatures. Another possibility is the onset of 3D LRO. In this case, a divergence should have been seen in the temperature dependencies of the spin-lattice relaxation rate  $1/T_1$  as well as in the spin-spin relaxation rate  $1/T_{2G}$ . While this is the case for  $\text{BaCuP}_2\text{O}_7$ , only a small increase of the relaxation rates is observed for  $\text{Sr}_2\text{Cu}(\text{PO}_4)_2$  and  $\text{Ba}_2\text{Cu}(\text{PO}_4)_2$ . A clear effect is observed in the temperature dependencies of  $K(T)$ ,  $1/T_1$ ,  $1/T_2$ , and lineshape for  $\text{BaCuP}_2\text{O}_7$  at 0.8 K. This establishes the onset of LRO at 0.8 K in  $\text{BaCuP}_2\text{O}_7$ . However, in the case of  $\text{Sr}_2\text{Cu}(\text{PO}_4)_2$  and  $\text{Ba}_2\text{Cu}(\text{PO}_4)_2$ , while a clear anomaly is seen in  $K(T)$  at low-temperature, only a weak anomaly is seen in  $1/T_1(T)$  and no significant changes were observed either in the low-temperature spectra or in  $1/T_2(T)$ . In summary, the presence or absence of LRO at

low-temperatures in  $\text{Sr}_2\text{Cu}(\text{PO}_4)_2$  and  $\text{Ba}_2\text{Cu}(\text{PO}_4)_2$ , can't be unambiguously established.

## B. Effect of chain ends on the NMR spectrum

From field-theory and Monte Carlo calculations, Eggert and Affleck<sup>29</sup> found that in case of half-integer spin chains, the local susceptibility near an open end of a finite chain has a large alternating component. This component appears in the form of staggered magnetization near chain ends, under the influence of an uniform field. This staggered moment has a maximum at a finite distance from the end and increases as  $1/T$  with decreasing temperature. Analytical expression for the spin susceptibility  $\chi(l)$  at site  $l$  were obtained which consist of the uniform ( $\chi_u$ ) and alternating ( $\chi_{alt}$ ) parts<sup>29</sup>  $\chi(l) = \chi_u(l) + (-1)^l \chi_{alt}(l)$ , where the uniform part is nearly constant and the alternating part is given by

$$\chi_{alt}(l) = \frac{aJ}{v} \frac{l}{\sqrt{(v/\pi T) \sinh(2\pi Tl/v)}} \quad (5)$$

where  $v = \pi J/2$  is the spin-wave velocity. The NMR spectrum represents the distribution function of NMR shift, which is equivalent to  $\chi_{alt}$ , and has the form  $g(x) = \sum_l f[x - (-1)^l \chi_{alt}(l)]$ , where  $f$  takes the form of a Lorentzian. This expression is valid for in-chain  $\text{Cu}^{2+}$  site. In our compounds,  $^{31}\text{P}$  is the probe nucleus, which is sensitive to two nearest neighbor  $\text{Cu}^{2+}$  ions belonging to one chain.  $^{31}\text{P}$  NMR line shape is then given by  $g(x) = \sum_l f[x - \{(-1)^l \chi_{alt}(l) + (-1)^{l+1} \chi_{alt}(l+1)\}]$ . Fig. 9 shows the simulated spectra for both Cu and P sites choosing  $f$  to be a Lorentzian with width 0.05.

For  $k_B T = J/33$ , at Cu site,  $\chi_{alt}$  has a maximum at  $l = 0.48J/T$ , which results in features in the spectra on either side of the central line. With increasing temperature these features on either side of the central peak disappear and  $\sqrt{T}(\frac{\Delta H}{2H_0})$  (where  $\Delta H$  is the width at the background and  $H_0$  is the field at the central peak) remain constant with temperature. This has been seen by Takigawa<sup>30</sup> in  $^{63}\text{Cu}$  NMR spectra of  $\text{Sr}_2\text{CuO}_3$ . However, the static effects of the staggered magnetization at the  $^{31}\text{P}$  site in our compounds are expected to be much weaker (Fig. 9) due to the near cancellation of the magnetization from the neighboring Cu sites.

Our low-temperature spectra for  $\text{Sr}_2\text{Cu}(\text{PO}_4)_2$  and  $\text{Ba}_2\text{Cu}(\text{PO}_4)_2$  show a single spectral

line without any shoulders on either sides of the central peak. This is in agreement with our expectations that we are not sensitive to chain-end effects in  $^{31}\text{P}$  NMR spectra of these compounds.

In low-field NMR on  $\text{BaCuP}_2\text{O}_7$ , a sudden increase of linewidth was observed below 0.8 K along with appearance of two shoulder-like features located symmetrically on either side of the central peak (Fig.6(d)). If these shoulder-like features come from the staggered magnetization of chain ends then, as discussed above,  $\sqrt{T}(\frac{\Delta H}{2H_0})$  should be temperature independent with the shoulders moving outwards at lower temperatures. But in  $\text{BaCuP}_2\text{O}_7$  the shoulder positions are temperature independent, suggesting that those features are not chain-end effects. Further, in case of a structural phase transition, symmetrically located features which become more intense as temperature is lowered are not expected. Our data are consistent with an alternating magnetization in the Cu chain. Further, the magnitude of this magnetization must have a maximum away from the chain end (so as to produce the symmetric features) and the location (site  $l_{max}$ ) of the maximum must not change with  $T$  (as the shoulder positions are temperature independent). As shown before, the chain-end induced effects are expected to be negligible at  $^{31}\text{P}$  site. The large effect seen here must stem from a magnetic transition possibly with exotic spin-order.

### C. Wave vector $\mathbf{q}$ - and temperature $T$ - dependence of $1/T_1$

In order to study the microscopic behavior of 1D HAF systems, it is useful to measure the temperature dependence of spin-lattice relaxation rate which yields information on the imaginary part of the dynamic susceptibility  $\chi(\mathbf{q}, \omega)$ . The spin-lattice relaxation rate, in general, is affected by both uniform ( $q = 0$ ) and staggered spin fluctuations ( $q = \pm\frac{\pi}{a}$ ). The uniform component leads to  $1/T_1 \propto T$ , while the staggered component gives  $1/T_1 = \text{constant}$ .<sup>7</sup> At the  $^{31}\text{P}$  sites,  $q$ -dependence of  $1/T_1$  can be expressed in terms of form factors as,

$$1/T_1 \propto \sum_q [A^2 \cos^2(qx)] \text{Im} \chi(q, \omega) \quad (6)$$

We are probing on the  $^{31}\text{P}$  nucleus, which is linked to the Cu spins via O(1) and O(2) as shown in Fig. 1. Since  $^{31}\text{P}$  is symmetrically located between the Cu ions, the antiferromagnetic fluctuations are filtered at the  $^{31}\text{P}$  site, provided the two hyperfine couplings are equal. However, contributions just slightly differing from  $q = \pi/a$  are apparently strong

enough and/or the two hyperfine couplings are unequal and result in a qualitative behavior expected when relaxation is dominated by fluctuations of the staggered susceptibility.

If one were to ignore the geometrical form factor completely, the relaxation rate due to staggered fluctuations can be calculated following the prescription of Barzykin<sup>16</sup>. He obtained the normalized dimensionless NMR spin-lattice relaxation rate at low-temperature  $(1/T_1)_{norm} = \frac{\hbar J}{A_{th}^2 T_1} \approx 0.3$ , where  $A_{th}$  is  $A(2\hbar\gamma/2\pi)$ . Assuming the fluctuations to be correlated,  $1/T_1$  can be written as  $1/T_1 = \frac{0.3}{\hbar J/A^2}$ . Using this expression,  $(1/T_1)$  at the  $^{31}\text{P}$  site was calculated to be about  $44 \text{ sec}^{-1}$ ,  $80 \text{ sec}^{-1}$  and  $47 \text{ sec}^{-1}$  whereas our experimental values are  $15 \text{ sec}^{-1}$ ,  $20 \text{ sec}^{-1}$  and  $25 \text{ sec}^{-1}$  for  $\text{Sr}_2\text{Cu}(\text{PO}_4)_2$ ,  $\text{Ba}_2\text{Cu}(\text{PO}_4)_2$ , and  $\text{BaCuP}_2\text{O}_7$  respectively in the  $1 \text{ K} \leq T \leq 10 \text{ K}$  range. The experimental values are clearly smaller than the theoretical ones due to the geometrical form factor. Further, a logarithmic increase of  $1/T_1$  is expected at low temperatures following<sup>16</sup>

$$(1/T_1)_{norm} = 2D \sqrt{\ln \frac{\Lambda}{T} + \frac{1}{2} \ln \left( \ln \frac{\Lambda}{T} \right)} \left( 1 + O \left[ \frac{1}{\ln^2 \frac{\Lambda}{T}} \right] \right) \quad (7)$$

where  $D = 1/(2\pi)^{3/2}$ ,  $\Lambda$  is the cutoff parameter given by  $2\sqrt{2\pi}e^{C+1}J$  and  $C (\simeq 0.5772157)$  is Euler's constant. In Fig. 10, we have plotted  $((1/T_1)/(1/T_1)_{T=10\text{K}})_{norm}$  calculated from equation 7 and the experimental results of the spin-lattice relaxation rate  $1/T_1$  for our compounds normalised by their values at 10 K, as a function of temperature. The qualitative temperature dependence of the experimental spin-lattice relaxation rate  $1/T_1$  agrees reasonably well with theoretical calculations in the constant region but below 0.5 K, the experimental increase in  $\text{Sr}_2\text{Cu}(\text{PO}_4)_2$  and  $\text{Ba}_2\text{Cu}(\text{PO}_4)_2$  is somewhat more than the logarithmic increase expected theoretically. However, complementary measurements are needed to fully understand this issue.

#### D. Spin-spin relaxation rate $1/T_{2G}$

Following the treatment of Sachdev<sup>7</sup> and Barzykin,<sup>16</sup> spin-spin relaxation is expected to follow a Gaussian behavior with a temperature dependence given by  $1/T_{2G} \propto 1/\sqrt{T}$ . Further, the spinon mediated spin-spin relaxation rate can be calculated<sup>16</sup> as follows. The normalized spin-spin relaxation rate is given by  $\left( \frac{\sqrt{T}}{T_{2G}} \right)_{norm} = \left( \frac{k_B T}{J} \right)^{1/2} \frac{\hbar J}{A^2 T_{2G}}$ . Dividing  $\left( \frac{1}{T_1} \right)_{norm}$  by  $\left( \frac{\sqrt{T}}{T_{2G}} \right)_{norm}$  and equating it to 1.8 (the value obtained from Ref. 16) one finds

that  $1/T_{2G} = \frac{44}{1.8} \left( \frac{J}{k_B T} \right)^{1/2}$ ,  $\frac{80}{1.8} \left( \frac{J}{k_B T} \right)^{1/2}$ , and  $\frac{47}{1.8} \left( \frac{J}{k_B T} \right)^{1/2}$ , respectively for  $\text{Sr}_2\text{Cu}(\text{PO}_4)_2$ ,  $\text{Ba}_2\text{Cu}(\text{PO}_4)_2$ , and  $\text{BaCuP}_2\text{O}_7$ . This leads to  $T_{2G}$  values 3.2 ms, 1.8 ms, and 3.6 ms in contrast to our experimental values  $269 \mu\text{s}$ ,  $255 \mu\text{s}$ , and  $207 \mu\text{s}$  respectively for  $\text{Sr}_2\text{Cu}(\text{PO}_4)_2$ ,  $\text{Ba}_2\text{Cu}(\text{PO}_4)_2$ , and  $\text{BaCuP}_2\text{O}_7$  at 1 K. These are almost three orders of magnitude smaller than the theoretically calculated values. Further, our experimental spin-spin relaxation rates are temperature independent. Clearly, in the present case, spinon mediated coupling does not contribute to spin-spin relaxation. On the other hand, an estimate of the nuclear dipole-dipole mediated relaxation  $\left( T_2 = \frac{r^3}{\gamma^2 \hbar} \right)$ , where  $r$  is the dipole-dipole distance would seem to explain the observed relaxation rates. This must be primarily because of the small exchange coupling in contrast to  $\text{Sr}_2\text{CuO}_3$  where  $J$  is an order of magnitude larger and spinon mediated Gaussian spin-spin relaxation rate has been observed.

## V. CONCLUSION

Our NMR and susceptibility measurements on  $\text{Sr}_2\text{Cu}(\text{PO}_4)_2$ ,  $\text{Ba}_2\text{Cu}(\text{PO}_4)_2$ , and  $\text{BaCuP}_2\text{O}_7$  show good agreement with the theory of 1D  $S = 1/2$  Heisenberg antiferromagnetic chains. NMR shift  $K$  as a function of temperature fitted well to the recent theoretical calculation by Johnston and the exchange interaction  $J/k_B$  is estimated to be 165 K, 151 K, and 108 K for  $\text{Sr}_2\text{Cu}(\text{PO}_4)_2$ ,  $\text{Ba}_2\text{Cu}(\text{PO}_4)_2$ , and  $\text{BaCuP}_2\text{O}_7$ , respectively. We observed a steep decrease of the NMR shift  $K(T)$  below  $T \simeq 0.003J/k_B$ ,  $0.0033J/k_B$ , and  $0.01J/k_B$  for  $\text{Sr}_2\text{Cu}(\text{PO}_4)_2$ ,  $\text{Ba}_2\text{Cu}(\text{PO}_4)_2$ , and  $\text{BaCuP}_2\text{O}_7$ , respectively. Low-field  $^{31}\text{P}$  NMR spectra of  $\text{BaCuP}_2\text{O}_7$  shows sudden appearance of broad humps on either side of the central peak for  $T < 0.8$  K, indicating the onset of LRO. The spin-lattice relaxation rate  $1/T_1$  was measured in a temperature range  $0.02 \text{ K} \leq T \leq 300 \text{ K}$ . No clear indication of any kind of magnetic ordering was seen in  $\text{Sr}_2\text{Cu}(\text{PO}_4)_2$  and  $\text{Ba}_2\text{Cu}(\text{PO}_4)_2$  from the  $1/T_1$  data, whereas a clear indication of magnetic ordering was observed at  $T \approx 0.8 \text{ K}$  ( $k_B T/J \approx 0.0074$ ) for  $\text{BaCuP}_2\text{O}_7$ . At low-temperature,  $1/T_1$  follows a nearly logarithmic increase for  $T \leq 0.5 \text{ K}$  for  $\text{Sr}_2\text{Cu}(\text{PO}_4)_2$  and  $\text{Ba}_2\text{Cu}(\text{PO}_4)_2$ , which is expected for a 1D  $S = 1/2$  HAF system. Though the transverse decays follow Gaussian behavior for all our samples, they result from dipole-dipole interaction rather than a spinon mediated interaction. Our experimental evidences on these compounds strongly reflect their low-dimensional nature making them one of the best 1D  $S = 1/2$  HAF systems that have been looked at so far.

## Acknowledgments

We would like to thank H.Alloul and J. Bobroff for some initial measurements and helpful discussions. We thank H.—A.Krug von Nidda for EPR measurements. One of us (AVM) would like to thank the Alexander von Humboldt foundation for financial support for the stay at Augsburg. This work was supported by the BMBF via VDI/EKM, FKZ 13N6917-A and by the Deutsche Forschungsgemeinschaft (DFG) through the Sonderforschungsbereich SFB 484 (Augsburg).

- 
- <sup>1</sup> F. D. M. Haldane, Phys. Rev. Lett. **50**, 1153 (1983).  
<sup>2</sup> H. A. Bethe Z. Phys. **71**, 205 (1931).  
<sup>3</sup> E. Lieb, T. D. Schultz, and D. C. Mattis, Ann. Phys. **16**, 407 (1961).  
<sup>4</sup> J. C. Bonner, M. E. Fisher, Phys. Rev. **135**, A640 (1964).  
<sup>5</sup> S. Eggert, I. Affleck, and M. Takahashi, Phys. Rev. Lett. **73**, 332 (1994).  
<sup>6</sup> D. C. Johnston, R. K. Kremer, M. Troyer, X. Wang, A. Klümper, S. L. Bud’ko, A. F. Panchula, and P. C. Canfield, Phys. Rev. B **61**, 9558 (2000).  
<sup>7</sup> S. Sachdev, Phys. Rev. B **50**, 13006 (1994).  
<sup>8</sup> A. W. Sandvik, Phys. Rev. B **52**, R9831 (1995).  
<sup>9</sup> D. Hone, C. Scherer, and F. Borsa, Phys. Rev. B **9**, 965 (1974).  
<sup>10</sup> P. M. Richards and F. Borsa, Solid State Commum. **15**, 135 (1974).  
<sup>11</sup> J. Chakhalian et.al., Physica B **326**, 422 (2003).  
<sup>12</sup> N. Motoyama, H. Eisaki, S. Uchida, Phys. Rev. Lett. **76**, 3212 (1996).  
<sup>13</sup> M. Takigawa, N. Motoyama, H. Eisaki, and S. Uchida, Phys. Rev. Lett. **76**, 4612 (1996).  
<sup>14</sup> M. Takigawa, O. A. Starykh, A. W. Sandvik, and R. R. P. Singh, Phys. Rev. B **56**, 13681 (1997).  
<sup>15</sup> K. R. Thurber, A. W. Hunt, T. Imai, and F. C. Chou, Phys. Rev. Lett. **87**, 247202 (2001).  
<sup>16</sup> V. Barzykin, Phys. Rev. B **63**, 140412 (2001).  
<sup>17</sup> A. A. Belik, A. P. Malakho, B. I. Lazoryak, and S. S. Khasanov, J. Solid State Chem. **163**, 121 (2002).  
<sup>18</sup> K.M.S. Etheredge, Shiou-Jyh Hwu, Inorganic Chemistry **35**, 1474 (1996).



- <sup>19</sup> A. Moqine, A. Boukhari and E. M. Holt, Acta Cryst. **C47**, 2294 (1991).
- <sup>20</sup> A. A. Belik, M. Azuma, and M. Takano, J. Solid State Chem. **177**, 883 (2004).
- <sup>21</sup> A. A. Belik, M. Azuma, and M. Takano, J. Magnetism and Magnetic Materials **272-276**, 937 (2004).
- <sup>22</sup> T. Ami et. al., Phys. Rev. B **51**, 5994 (1995).
- <sup>23</sup> J. Das, A.V. Mahajan, J. Bobroff, H. Alloul, F. Alet, E. S. Sorensen, Phys. Rev. B **69**, 144404 (2004).
- <sup>24</sup> P.W. Selwood, Magnetochemistry, Interscience, New York, 1956.
- <sup>25</sup> L. E. Drain, Proc. Phys. Soc., **80**, 1380 (1962).
- <sup>26</sup> A slightly higher  $1/T_1$  at low-field is compatible with the results for  $\text{Sr}_2\text{CuO}_3$ , where it was explained by Takigawa<sup>13</sup> based on spin-diffusion.
- <sup>27</sup> A similar decrease was observed in  $^{17}\text{O}$  NMR shift of  $\text{Sr}_2\text{CuO}_3$  below  $k_B T/J \sim 0.015$ <sup>15</sup>. In that case, it was suggested that the decrease was unrelated to magnetic ordering which took place at  $k_B T/J \sim 0.002$  and might be a general feature of  $S = 1/2$  1D HAF systems, so far not predicted theoretically.
- <sup>28</sup> Using  $\chi_{spin}(T=0)$  from Ref. 2,  $K(T=0) = K_0 + \frac{Ag^2\mu_B}{k_B(J/k_B)} \frac{1}{\pi^2}$ .
- <sup>29</sup> S. Eggert and I. Affleck, Phys. Rev. Lett. **75**, 934 (1995).
- <sup>30</sup> M. Takigawa, N. Motoyama, H. Eisaki and S. Uchida, Phys. Rev. B **55**, 14129 (1997).

### Figure Captions

FIG. 1 Schematic diagram of  $[\text{Cu}(\text{PO}_4)_2]_\infty$  linear chains (a) propagating along  $b$ -direction for  $(\text{Ba}/\text{Sr})_2\text{Cu}(\text{PO}_4)_2$  and (b) along the  $c$ -direction for  $\text{BaCuP}_2\text{O}_7$ . The arrows show the direction of chains while the possible interaction paths are shown by solid lines between atoms.

FIG. 2 X-ray diffraction pattern (Intensity vs.  $2\theta$ ) for (a)  $\text{Sr}_2\text{Cu}(\text{PO}_4)_2$ , (b)  $\text{Ba}_2\text{Cu}(\text{PO}_4)_2$ , and (c)  $\text{BaCuP}_2\text{O}_7$ . Miller indices are not shown in order to maintain the clarity of the figures. Impurity peaks are marked by asterisks.

FIG. 3 Magnetic susceptibility ( $M/H$ ) vs. temperature  $T$  for (a)  $\text{Sr}_2\text{Cu}(\text{PO}_4)_2$ , (b)  $\text{Ba}_2\text{Cu}(\text{PO}_4)_2$ , and (c)  $\text{BaCuP}_2\text{O}_7$  in an applied field of 5 kG. The solid lines are best fits of the data to Eq. 1. Insets of (a) and (b) display the comparison of the magnetic susceptibility for as-prepared and reduced samples at lower temperatures. Susceptibility variations as a function of  $\frac{1}{T}$  are shown to demonstrate the lowering of Curie term on reduction.

FIG. 4  $^{31}\text{P}$  shift  $K$  vs. temperature  $T$  for (a)  $\text{Sr}_2\text{Cu}(\text{PO}_4)_2$ , (b)  $\text{Ba}_2\text{Cu}(\text{PO}_4)_2$ , and (c)  $\text{BaCuP}_2\text{O}_7$ . The solid lines are fits of Eq. 2 in the temperature range,  $10 \text{ K} \leq T \leq 300 \text{ K}$  and then extrapolated down to 0.01 K. Inset shows  $K$  vs.  $T$  on a logarithmic temperature scale for improved visualisation of the low- $T$  data.

FIG. 5  $^{31}\text{P}$  shift  $K$  vs. spin susceptibility  $\chi_{\text{Spin}}$  for  $\text{BaCuP}_2\text{O}_7$ . The solid line shows the linear fit.

FIG. 6 Low-field ( $H \simeq 4 \text{ kG}$ )  $^{31}\text{P}$  NMR spectra at different temperatures  $T$  for (a)  $\text{Sr}_2\text{Cu}(\text{PO}_4)_2$  and (b)  $\text{Ba}_2\text{Cu}(\text{PO}_4)_2$ . The insets of (a) and (b) contain the high-field and low-field spectra at 1 K. (c) and (d) show high-field and low-field spectra, respectively, for  $\text{BaCuP}_2\text{O}_7$  at various temperatures below 1 K, showing the sudden change in line width there.

FIG. 7 Spin-lattice relaxation rate  $1/T_1$  (both high and low fields) vs. temperature  $T$  for (a)  $\text{Sr}_2\text{Cu}(\text{PO}_4)_2$ , (b)  $\text{Ba}_2\text{Cu}(\text{PO}_4)_2$ , and (c)  $\text{BaCuP}_2\text{O}_7$ . In the inset of (a), the high-field magnetization recoveries are plotted as a function of pulse separation  $t$  and the solid line is a single-exponential fit for  $\text{Sr}_2\text{Cu}(\text{PO}_4)_2$ . The inset of (b) displays the relaxation rate data for  $\text{Ba}_2\text{Cu}(\text{PO}_4)_2$  on a linear temperature scale. In the inset of (c), the low-field magnetization recoveries are plotted as a function of pulse separation  $t$  at 1 K and 2 K. The 1 K data are fitted to double exponential (Eq. 3), while 2 K data are fitted to single exponential.

FIG. 8 Spin-echo decays are plotted as a function of  $t^2$  at two different temperatures for (a)  $\text{Sr}_2\text{Cu}(\text{PO}_4)_2$ , (b)  $\text{Ba}_2\text{Cu}(\text{PO}_4)_2$ , and (c)  $\text{BaCuP}_2\text{O}_7$ . The solid lines show the fitting to a Gaussian function (Eq. 4). In the insets,  $1/T_{2G}$  is plotted as a function of temperature  $T$ .

FIG. 9 Distribution function  $g(x)$  which represents the NMR spectrum is plotted for (a) Cu site and (b) P sites. In the insets of (a) and (b),  $(-1)^l \chi_{\text{alt}}(l)$  and  $(-1)^l \chi_{\text{alt}}(l) + (-1)^{l+1} \chi_{\text{alt}}(l+1)$  respectively are plotted as a function of the site index  $l$  from the chain end at two different temperatures.

FIG. 10 Normalized experimental data (open symbols) as well as theoretical curve (solid line) of  $(1/T_1)_{\text{norm}}$  are plotted vs.  $k_B T/J$  for  $\text{Sr}_2\text{Cu}(\text{PO}_4)_2$ ,  $\text{Ba}_2\text{Cu}(\text{PO}_4)_2$ , and  $\text{BaCuP}_2\text{O}_7$  at low temperatures,  $0.1 \text{ K} \leq T \leq 10 \text{ K}$ . The data and the theoretical curves have been scaled to 1 at 10 K.

## Table Captions

TABLE I. Values of the parameters ( $\chi_0$ ,  $C$ ,  $\theta$ , and  $J/k_B$ ) obtained by fitting the bulk susceptibility to Eq. 1 to for each of the three samples.

TABLE II. Values of the parameters ( $K_0$ ,  $A$ , and  $J/k_B$ ) obtained by fitting the NMR shift data to Eq. 2 in the temperature range,  $10 \text{ K} \leq T \leq 300 \text{ K}$  for each of the three samples.

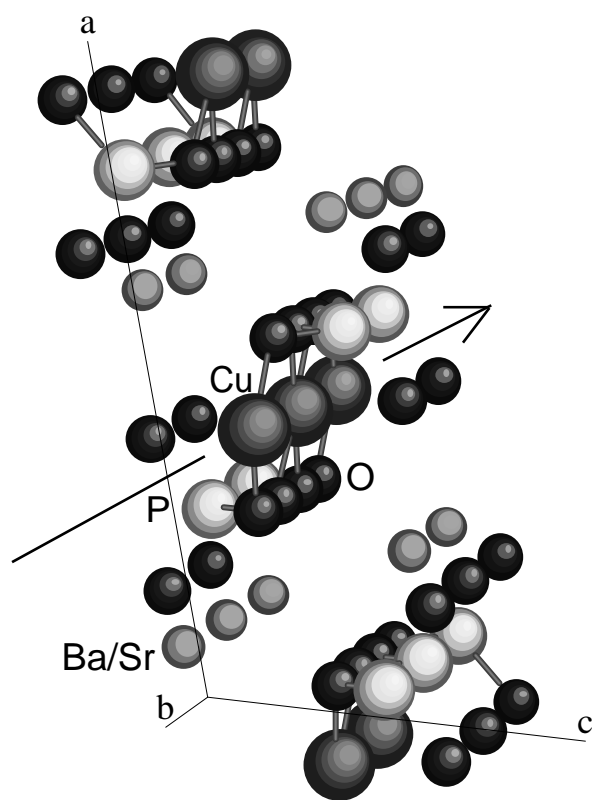


Fig. 1(a), R.Nath et al.

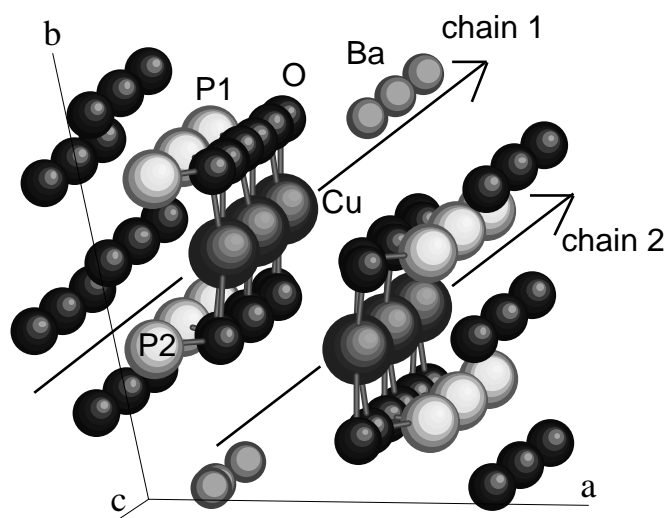


Fig. 1(b), R.Nath et al.

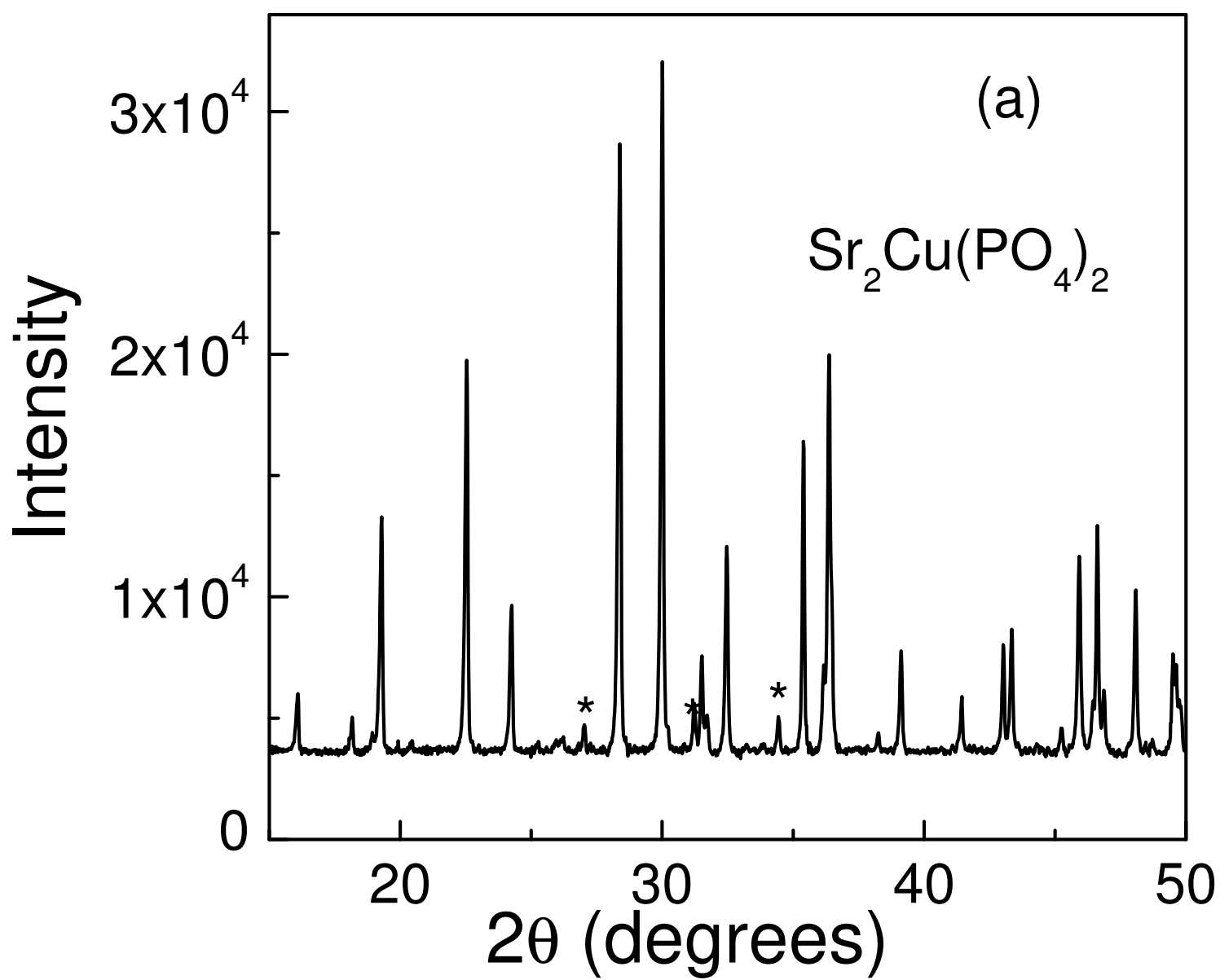


Fig. 2 (a), R. Nath et al.

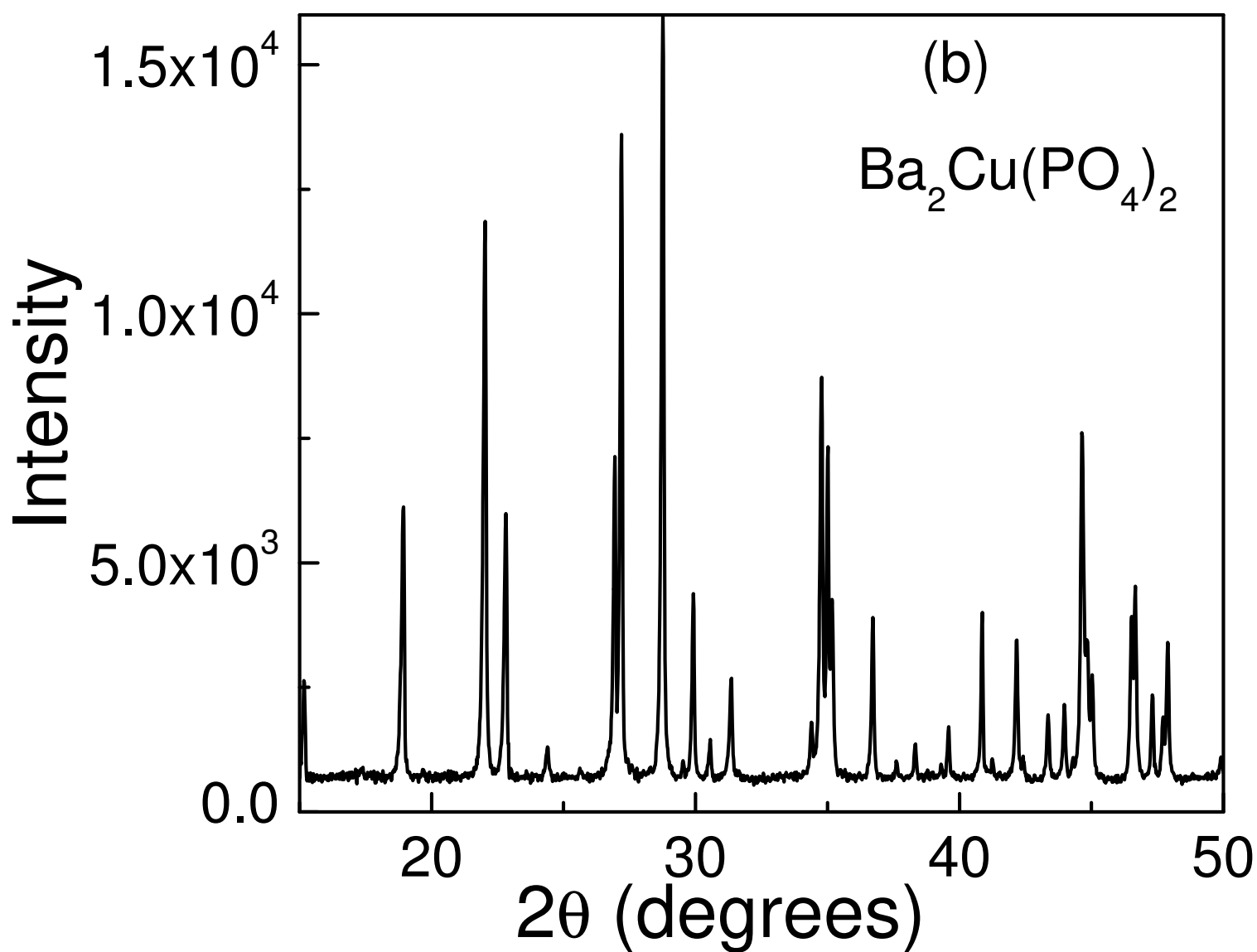


Fig. 2 (b), R. Nath et al.

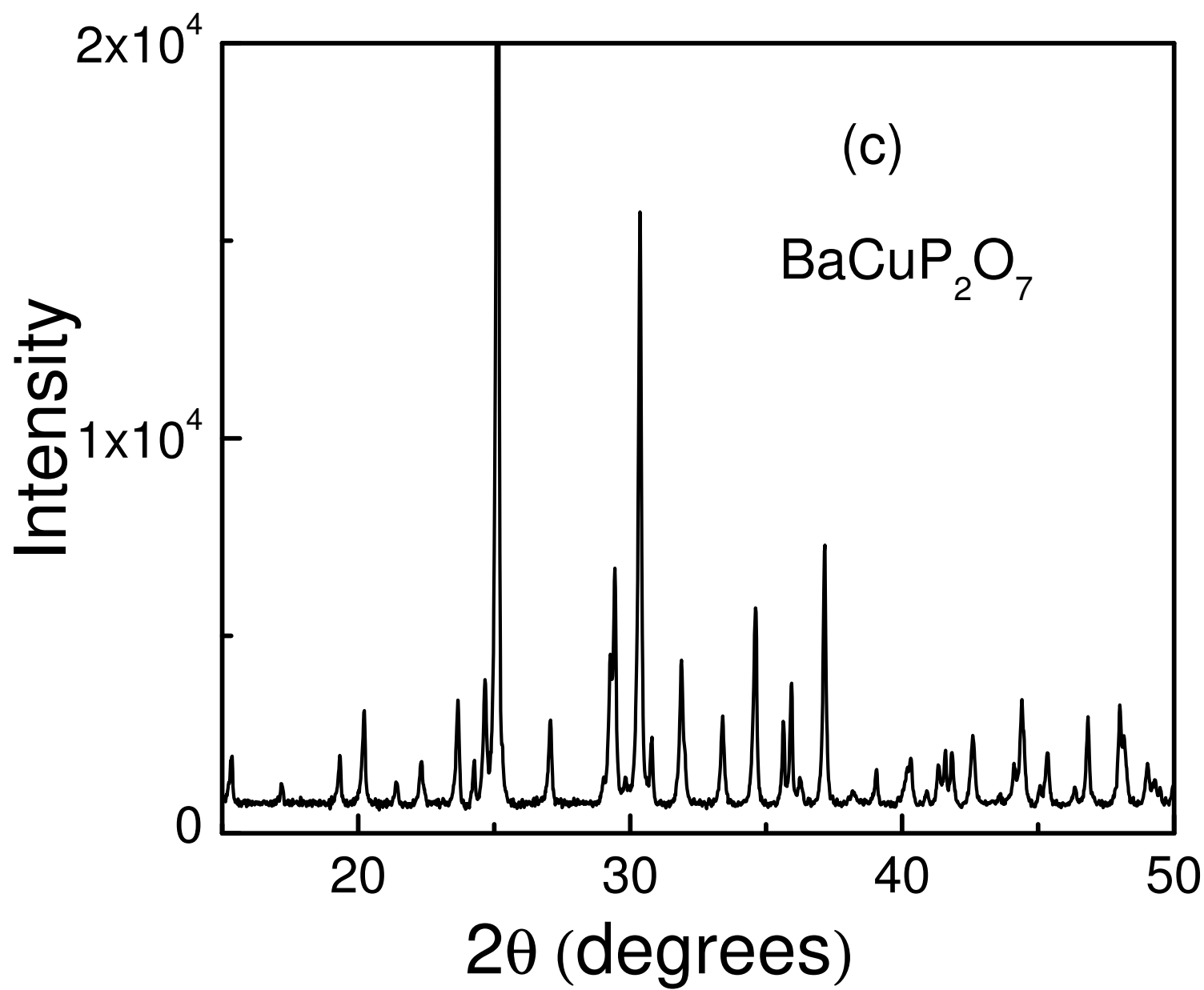


Fig. 2 (c), R. Nath et al.



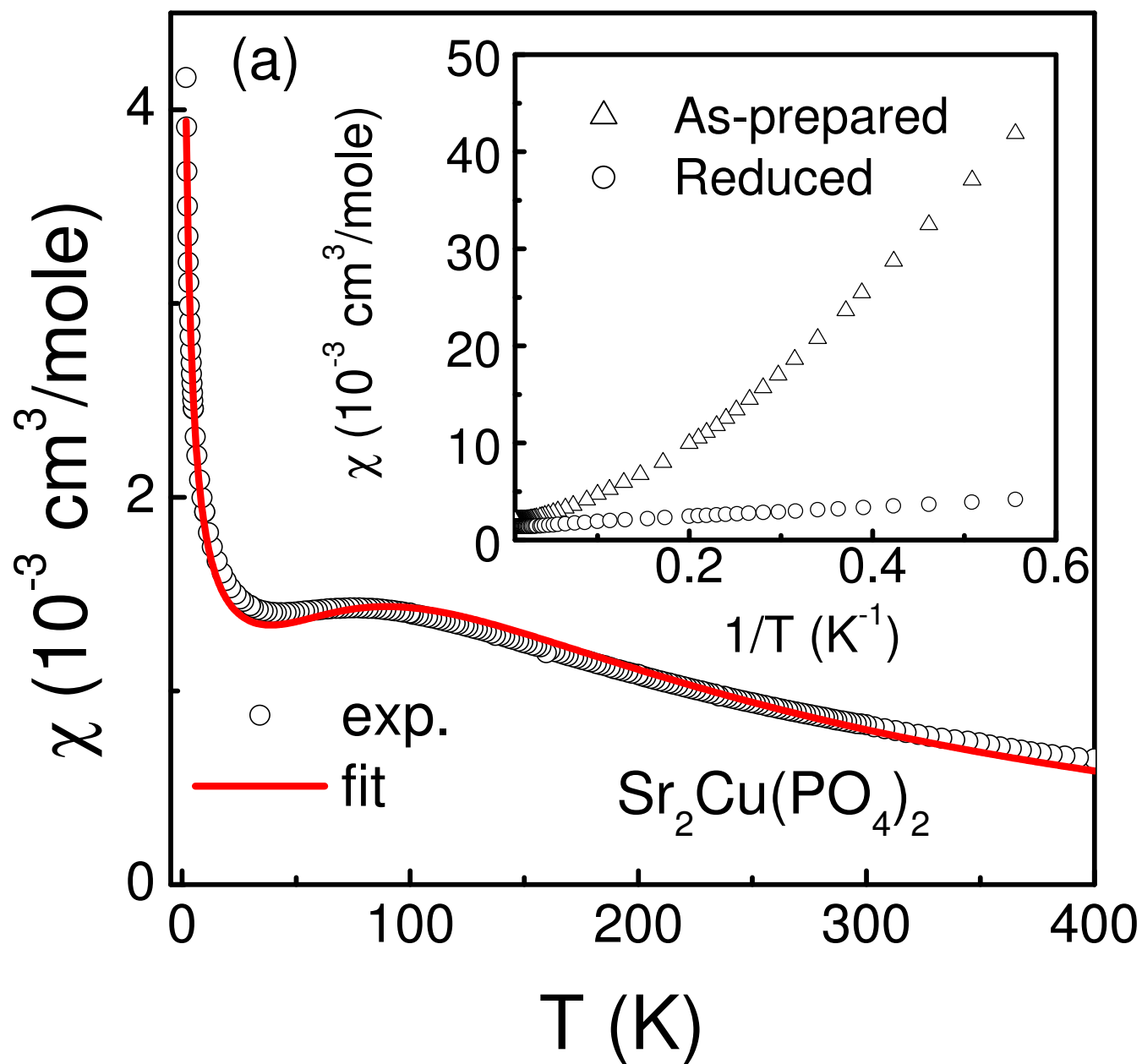


Fig. 3 (a), R. Nath et al.

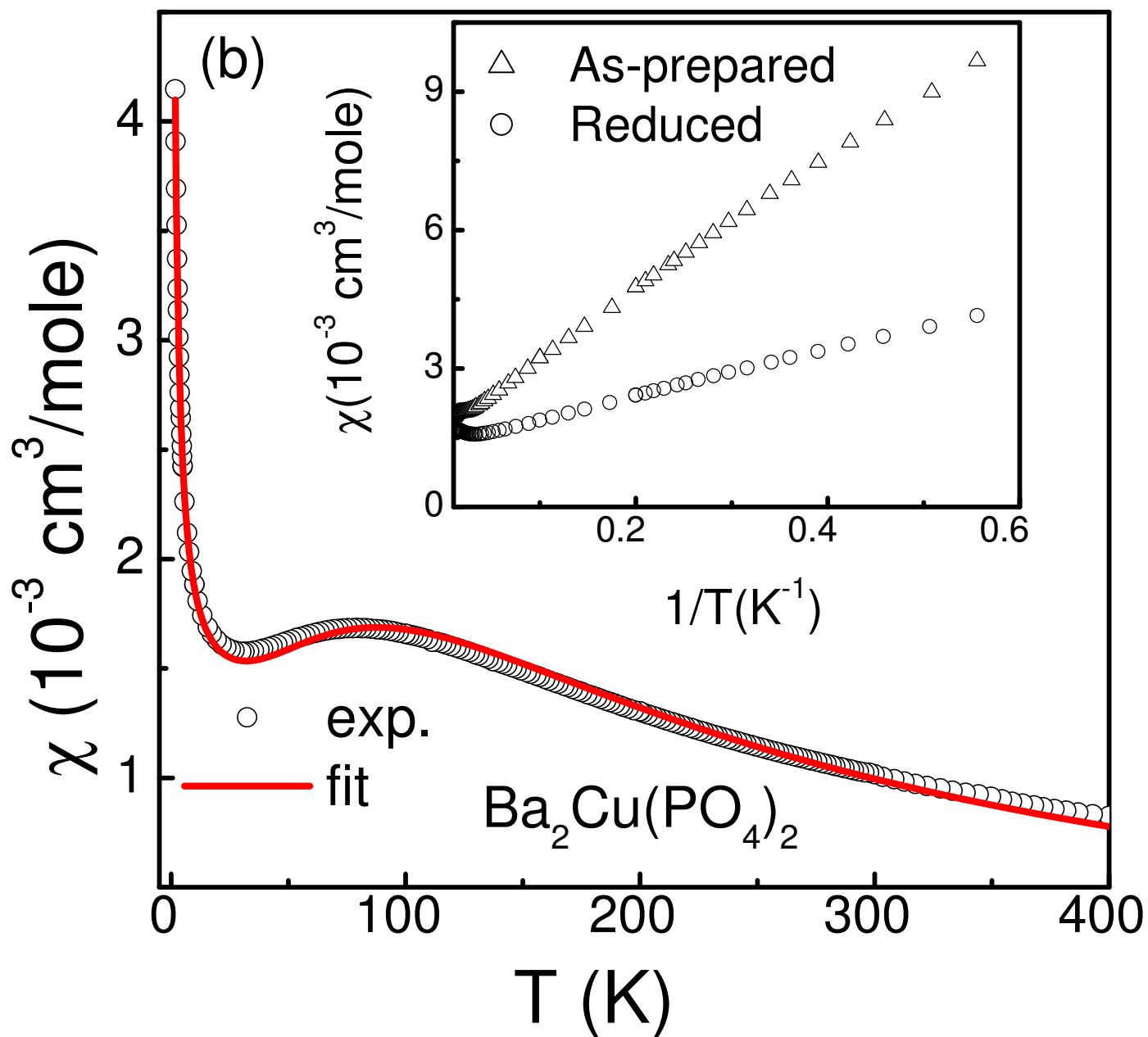


Fig. 3 (b), R. Nath et al.

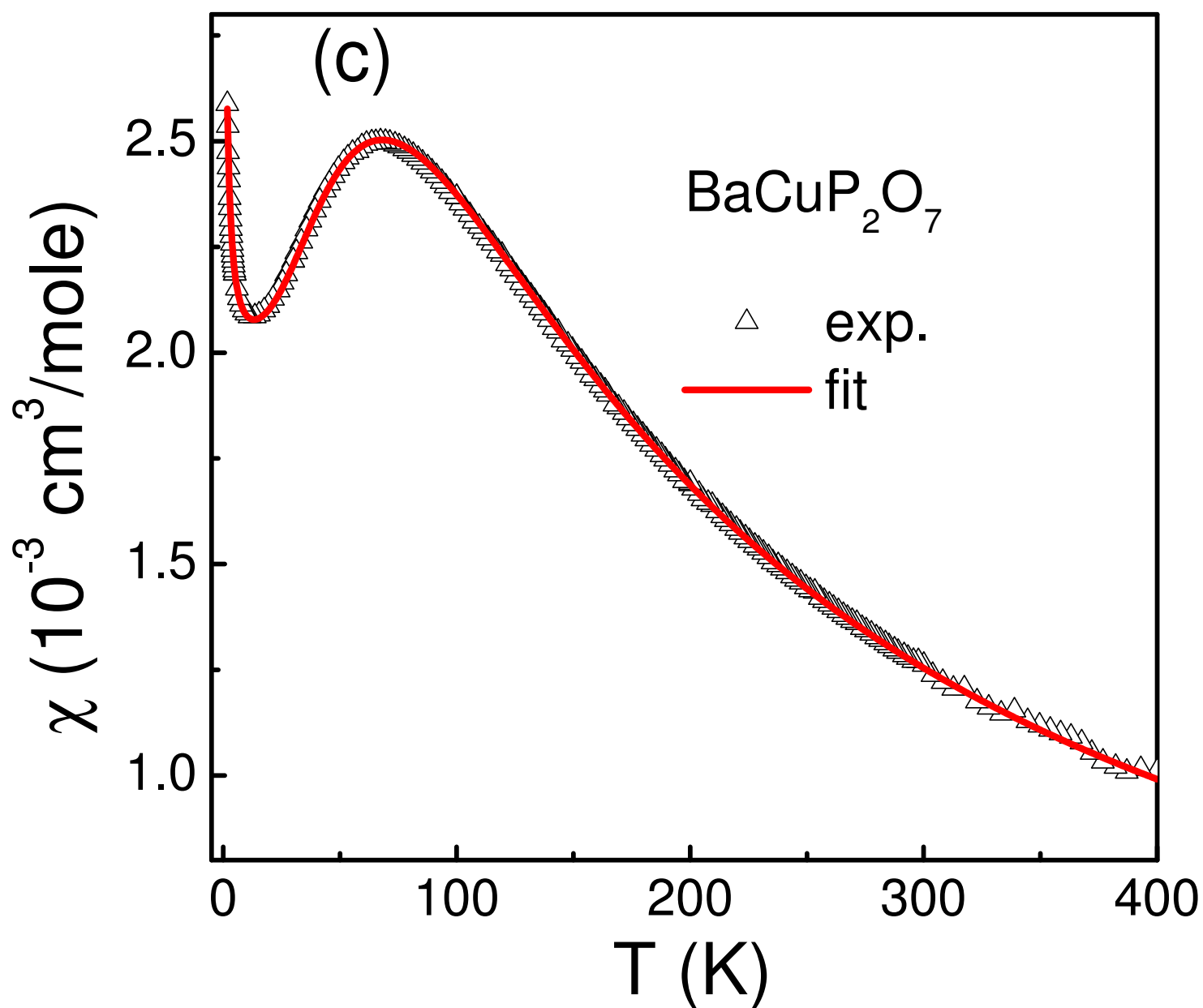


Fig. 3 (c), R. Nath et al.

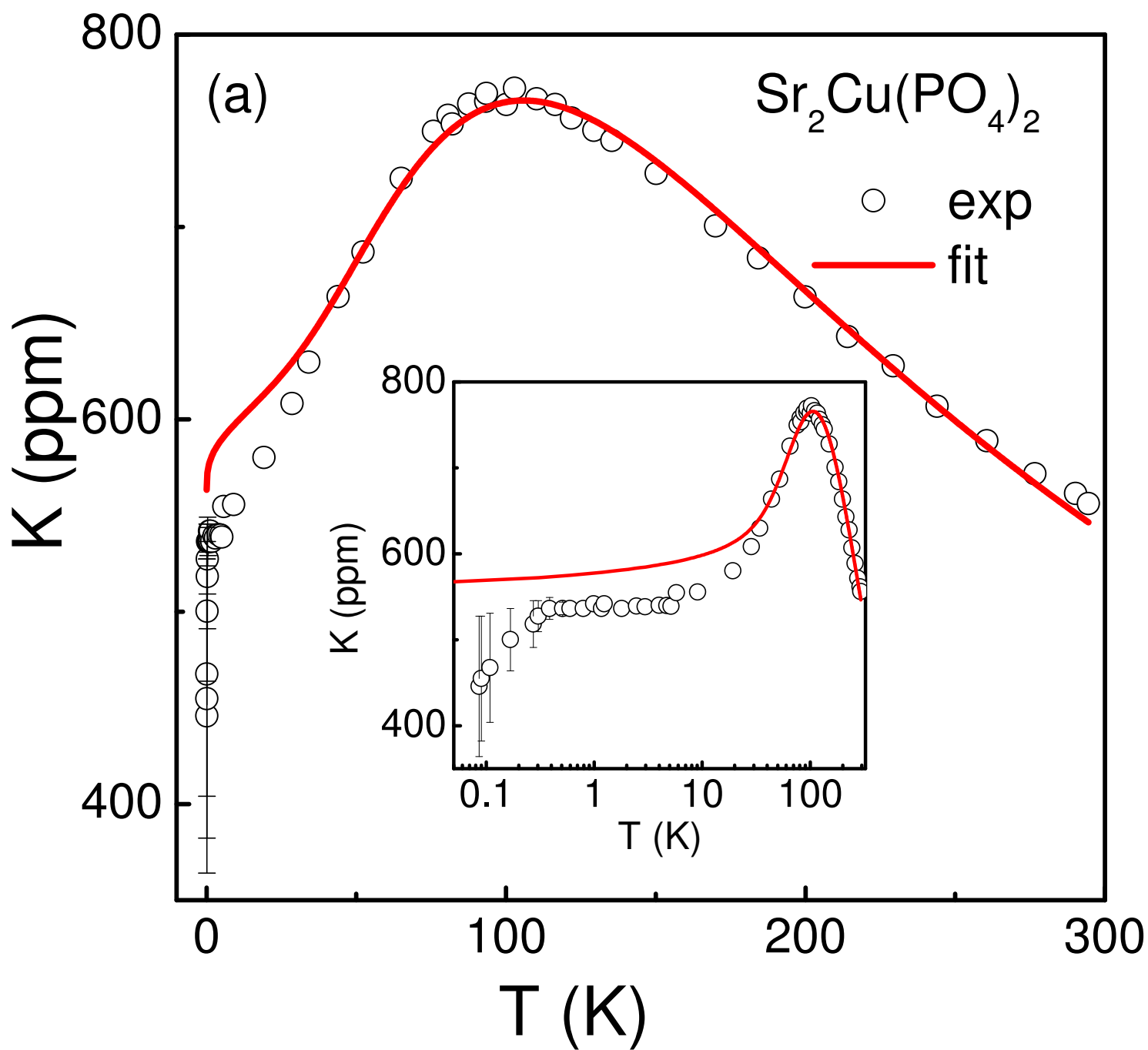


Fig. 4 (a), R. Nath et al.

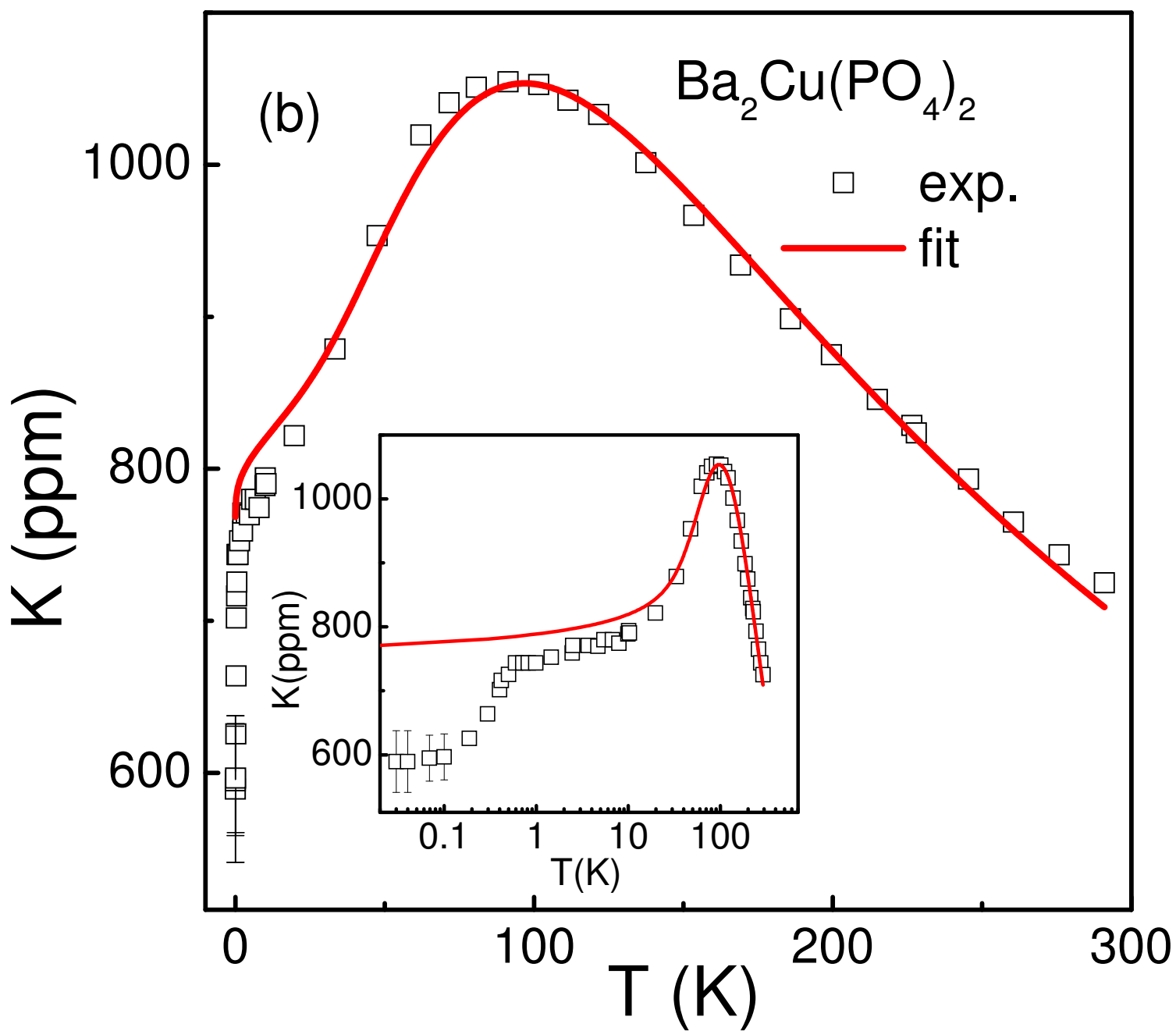


Fig. 4 (b), R. Nath et al.

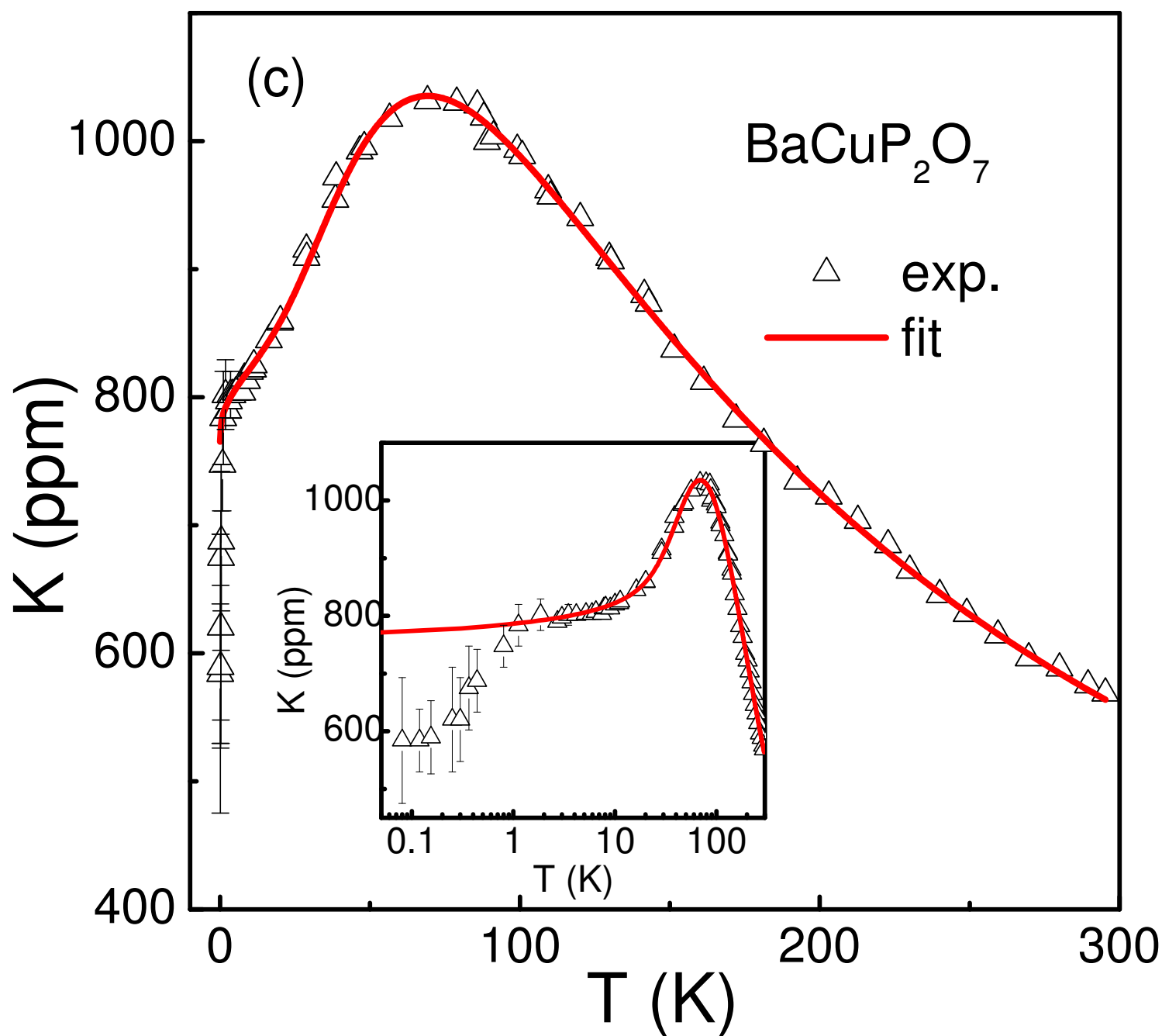


Fig. 4 (c), R. Nath et al.

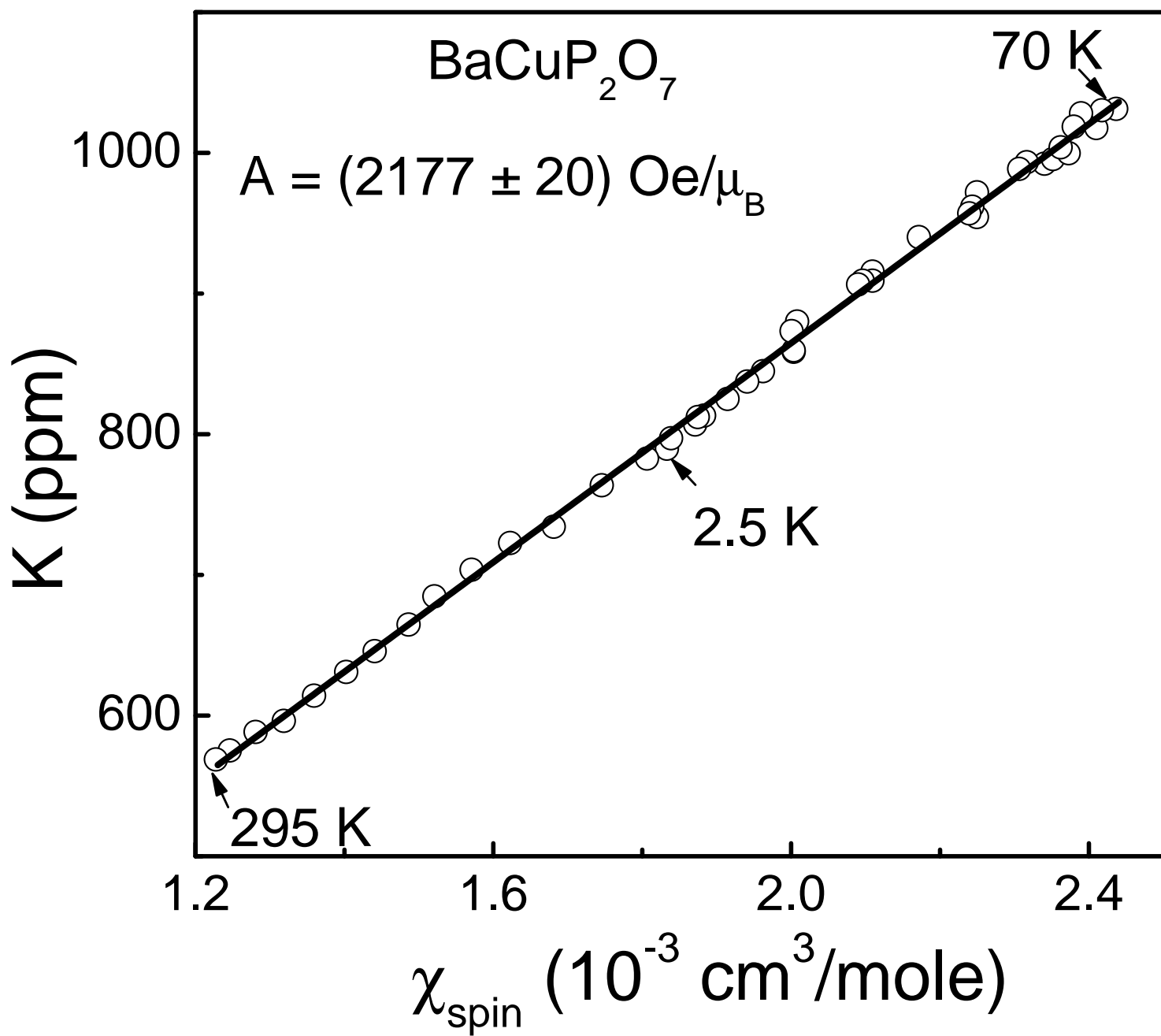


Fig. 5, R. Nath et al.

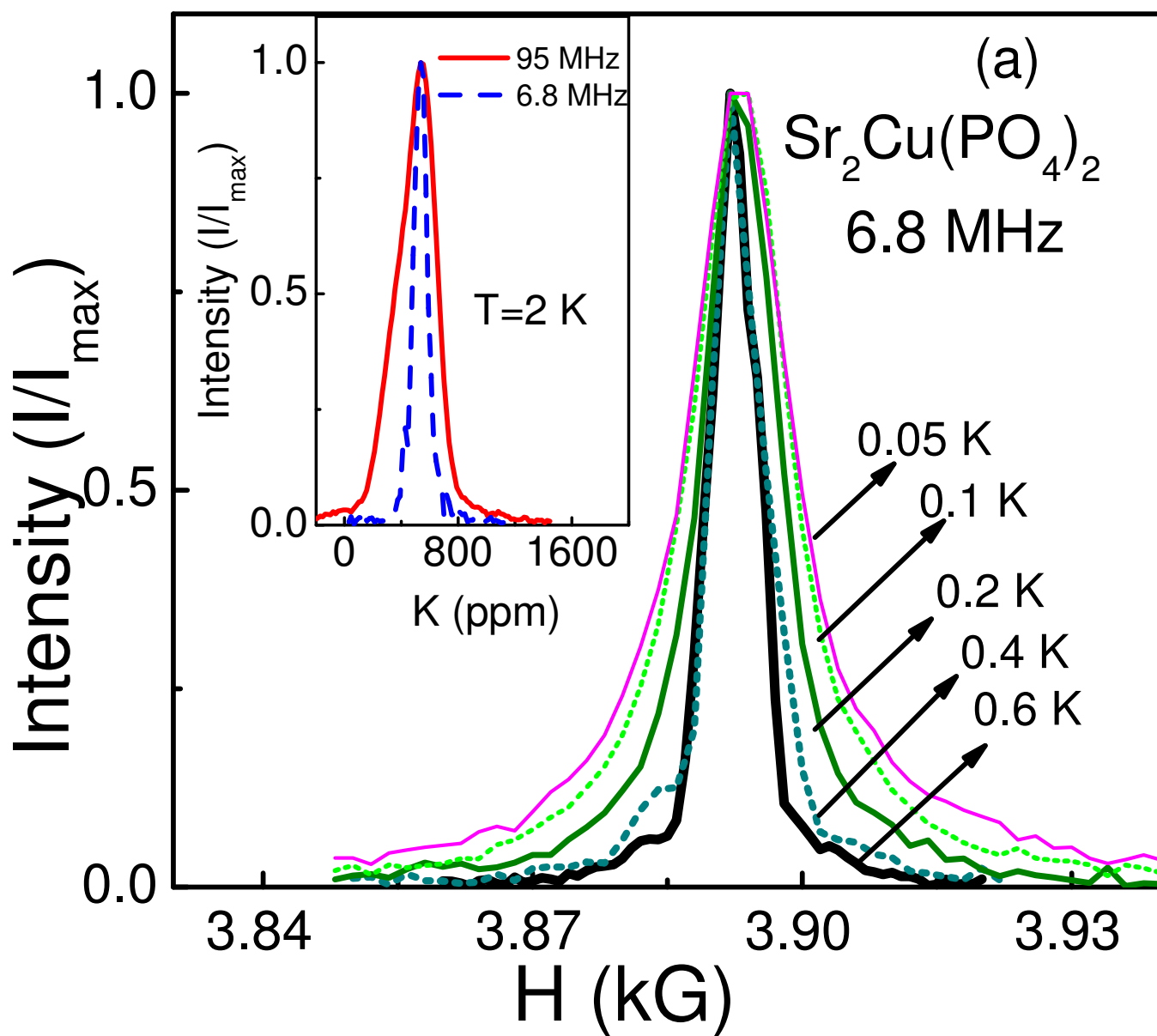


Fig. 6 (a), R. Nath et al.



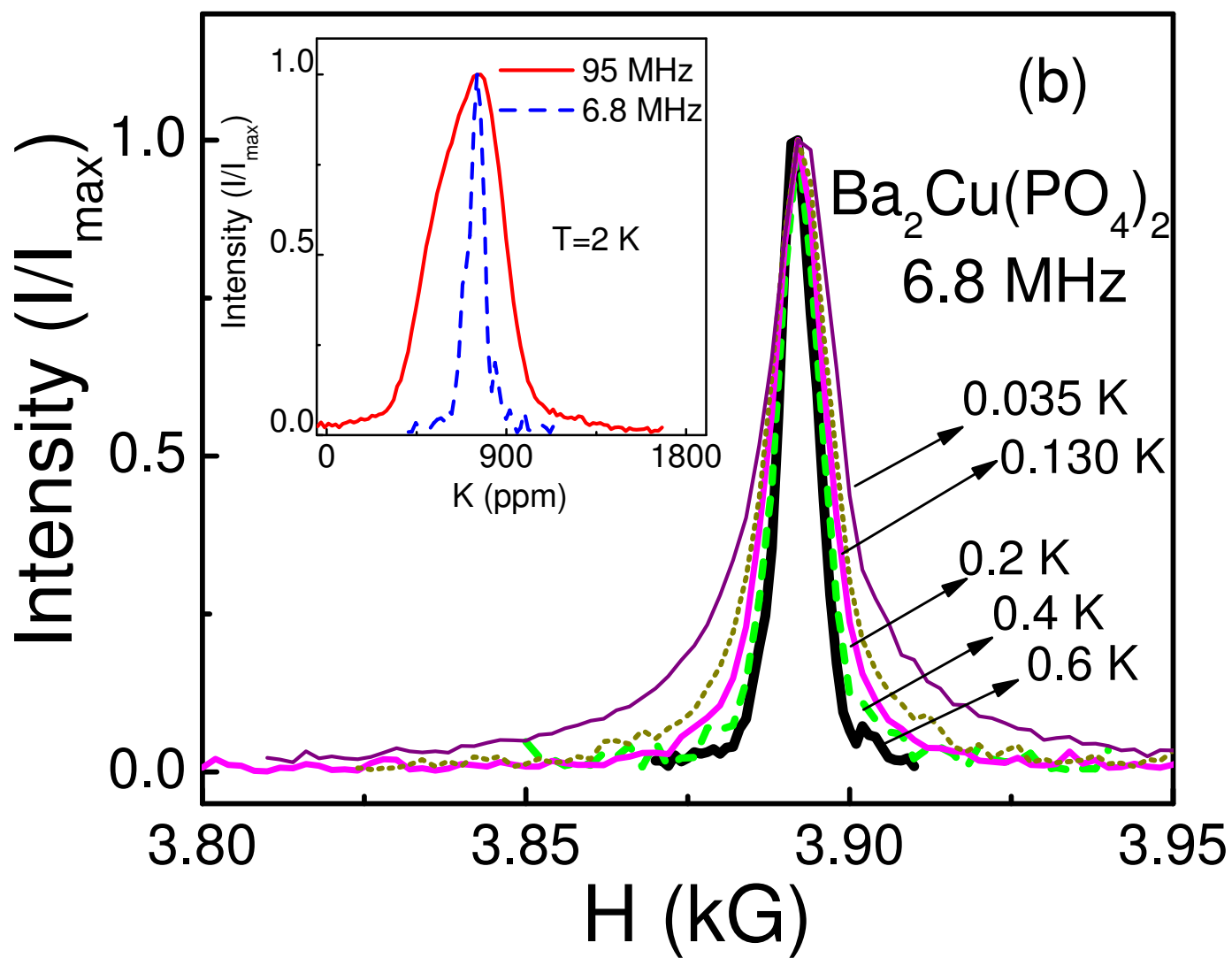


Fig. 6 (b), R. Nath et al.

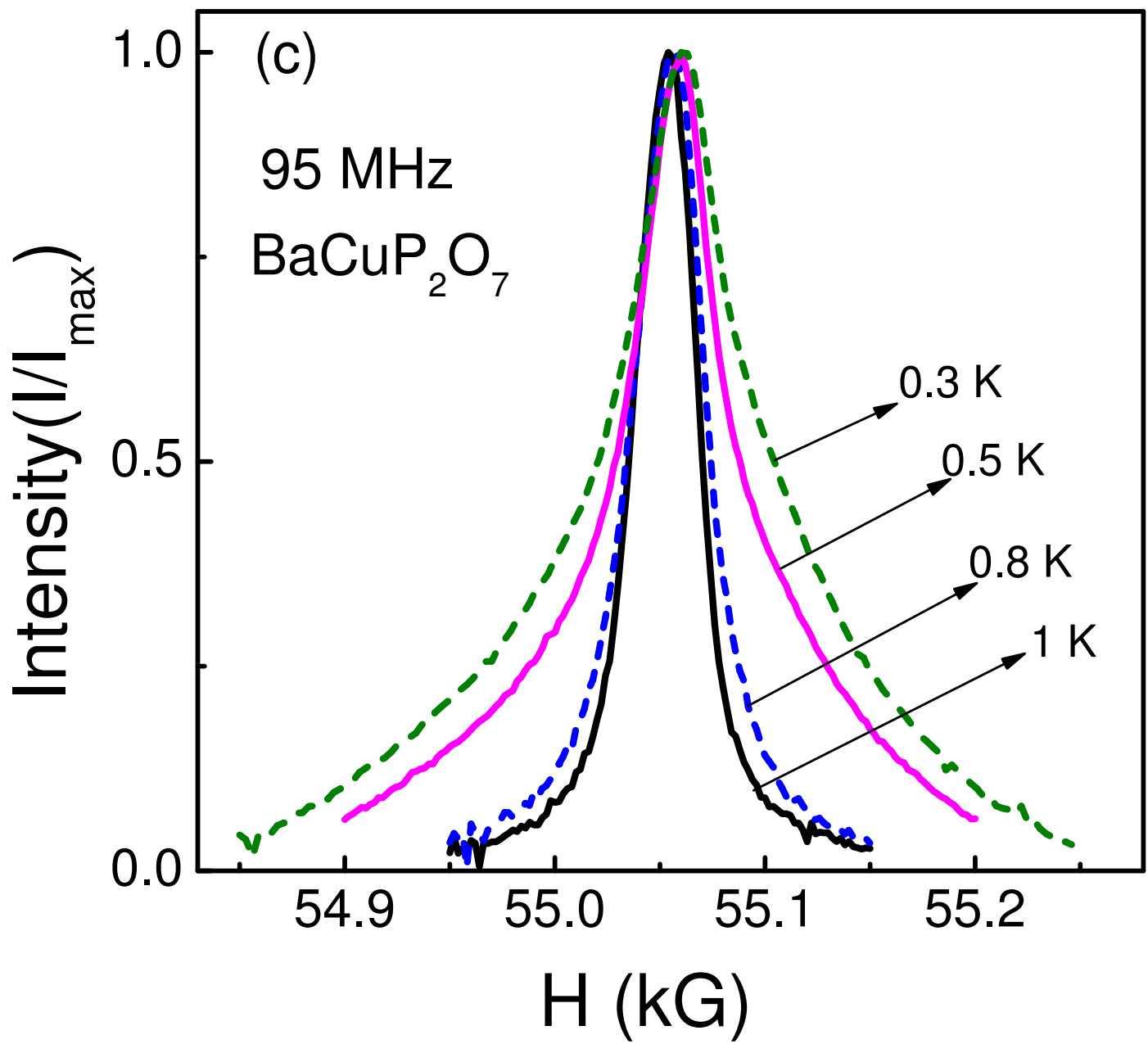


Fig. 6 (c), R. Nath et al.

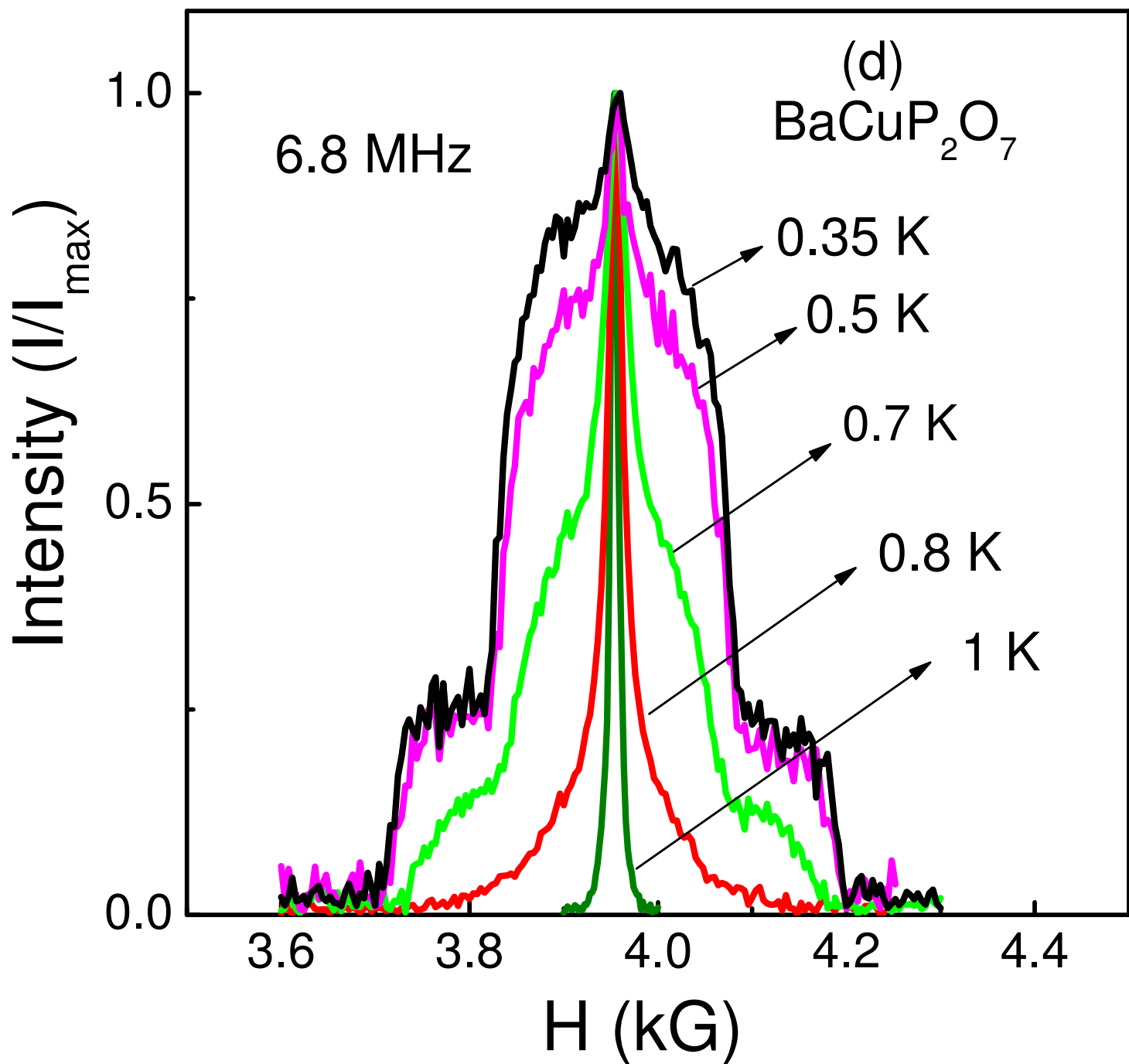


Fig. 6 (d), R. Nath et al.

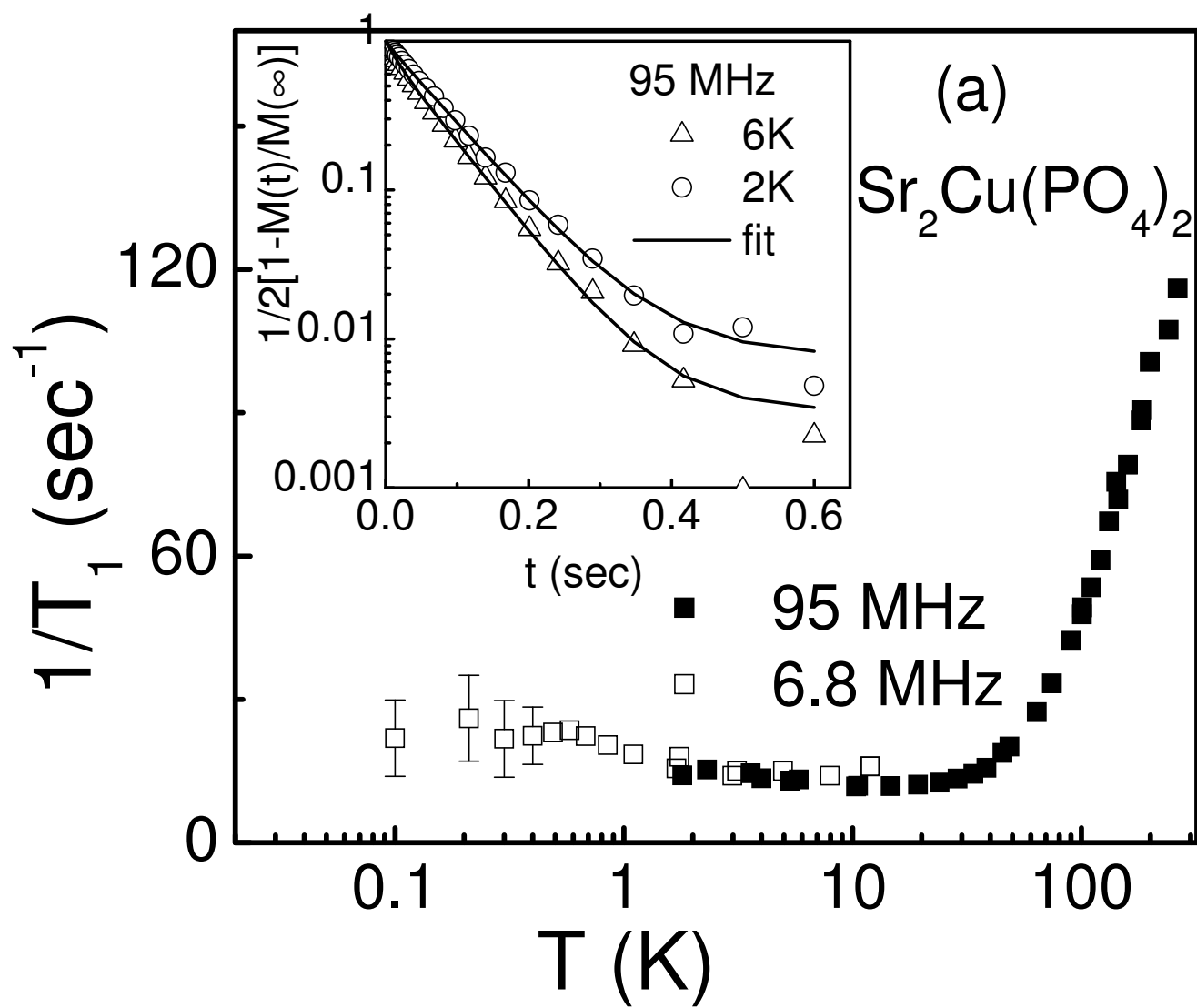


Fig. 7 (a), R. Nath et al.

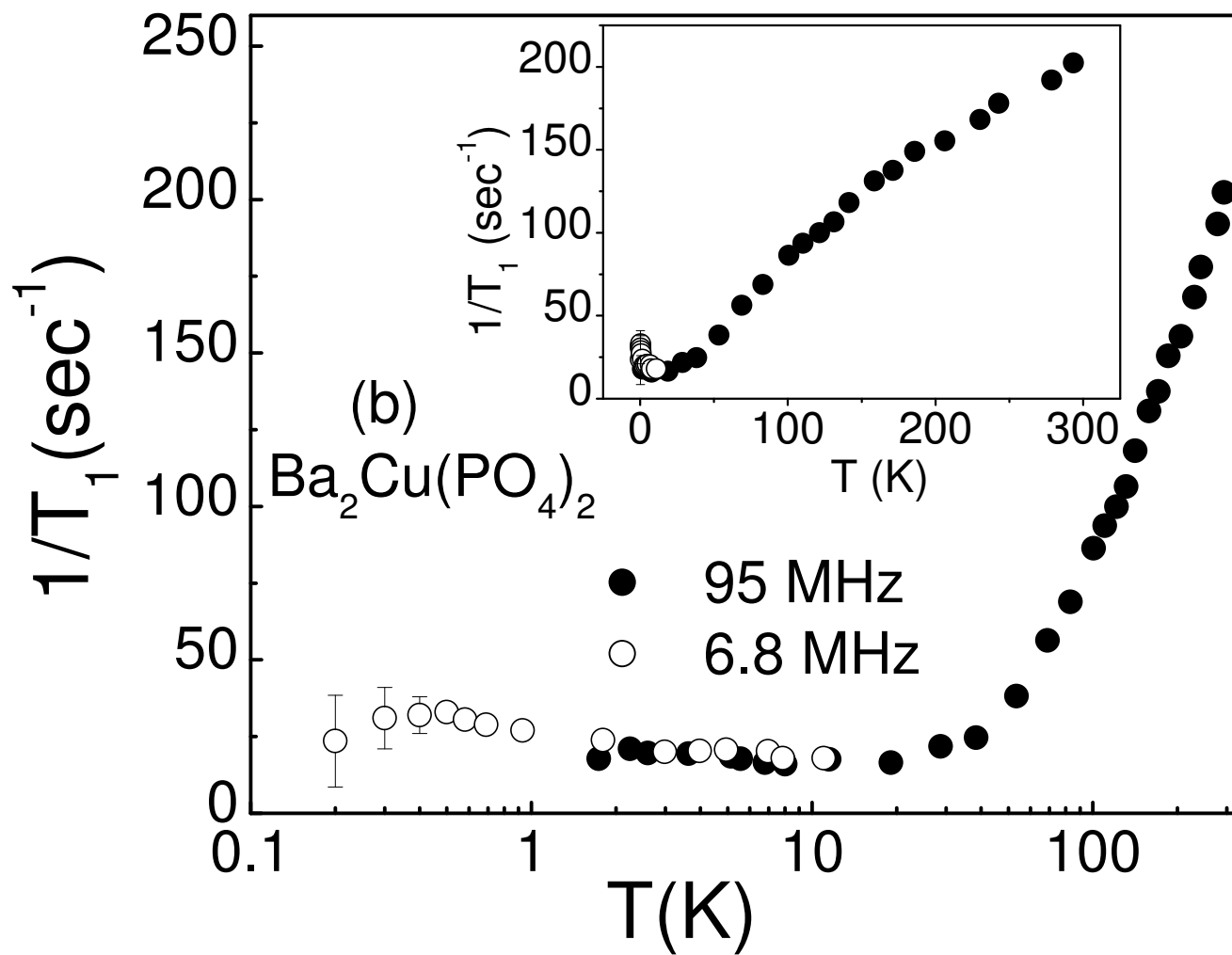


Fig. 7 (b), R. Nath et al.

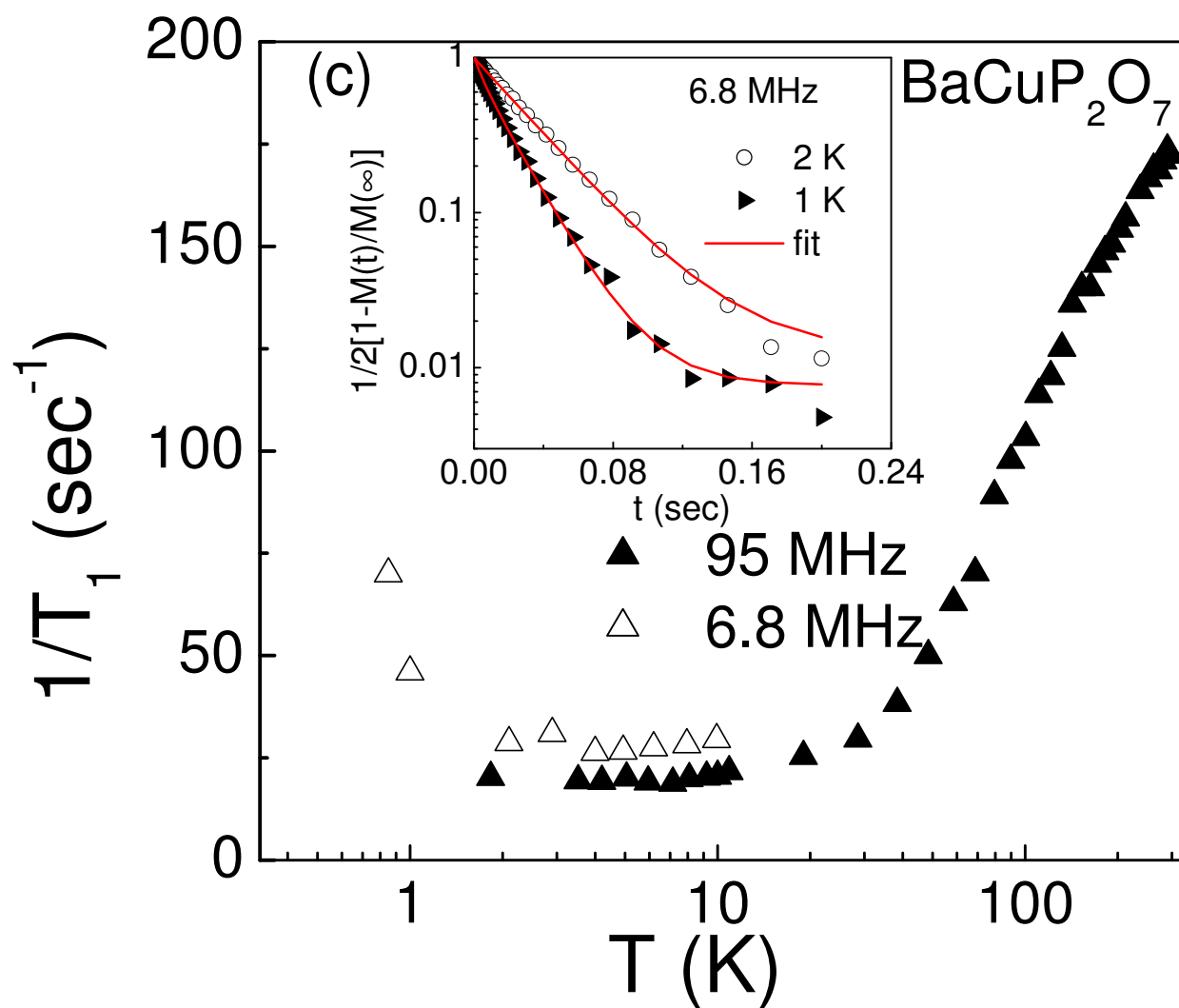


Fig. 7 (c), R. Nath et al.

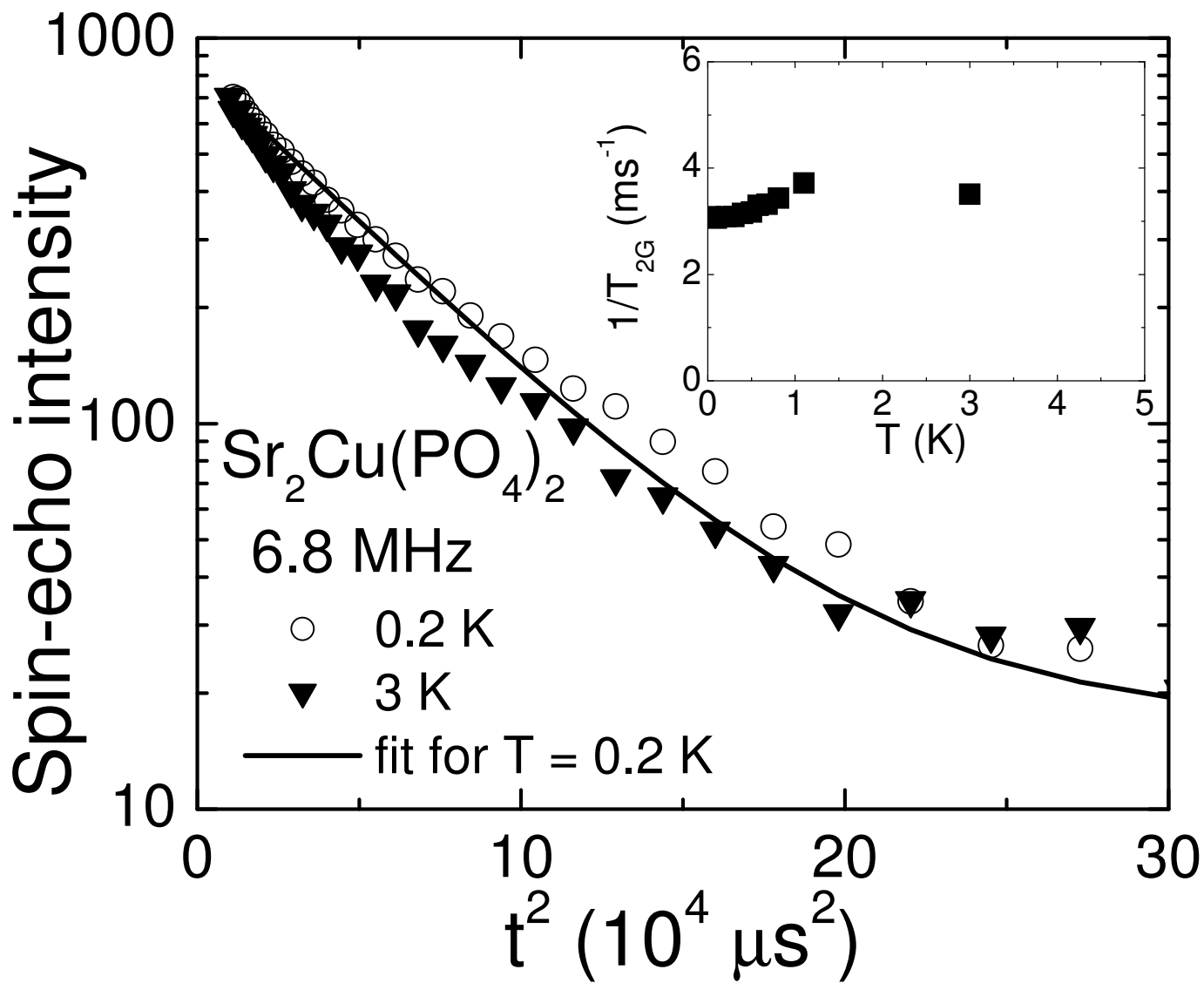


Fig. 8 (a), R. Nath et al.

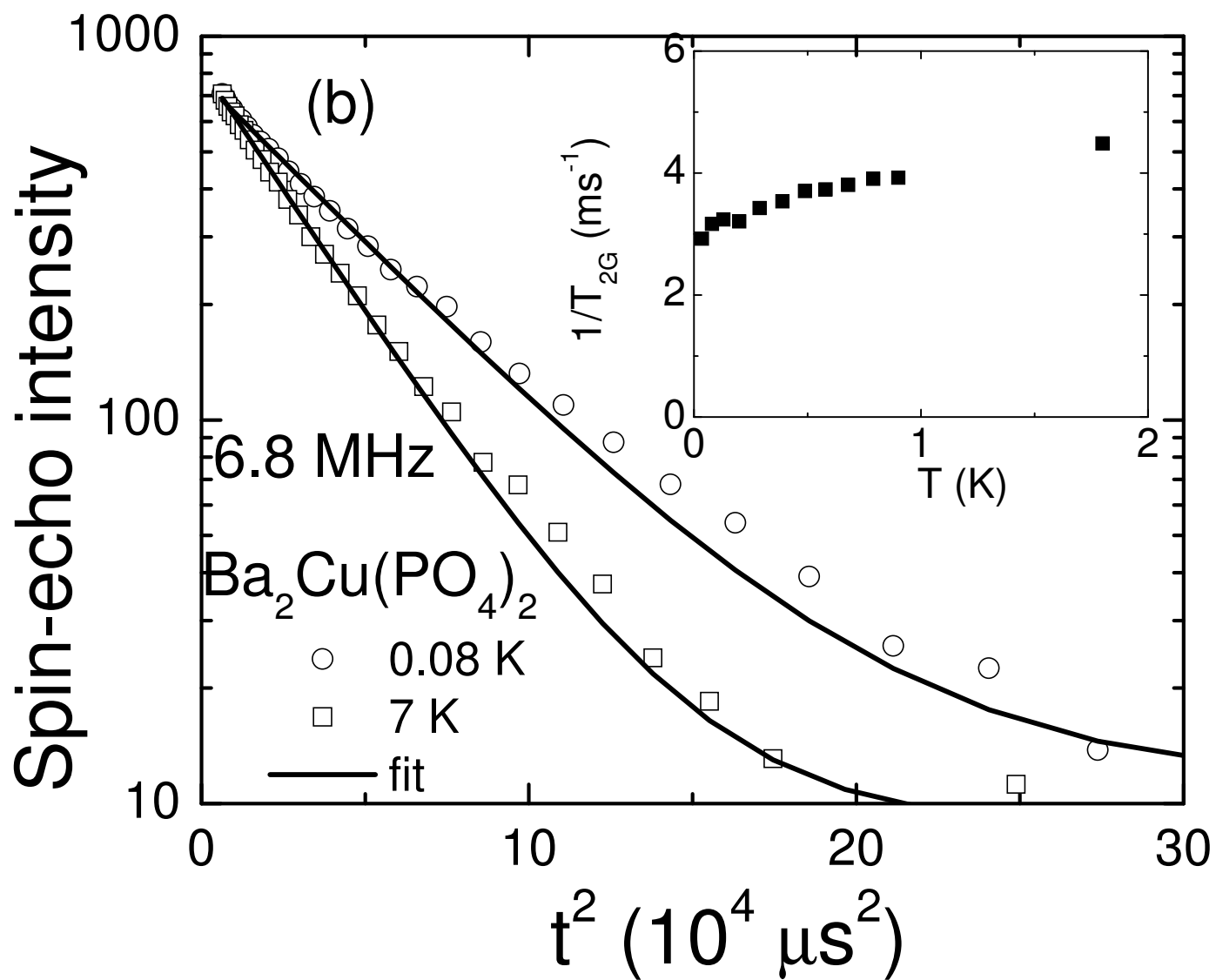


Fig. 8 (b), R. Nath et al.



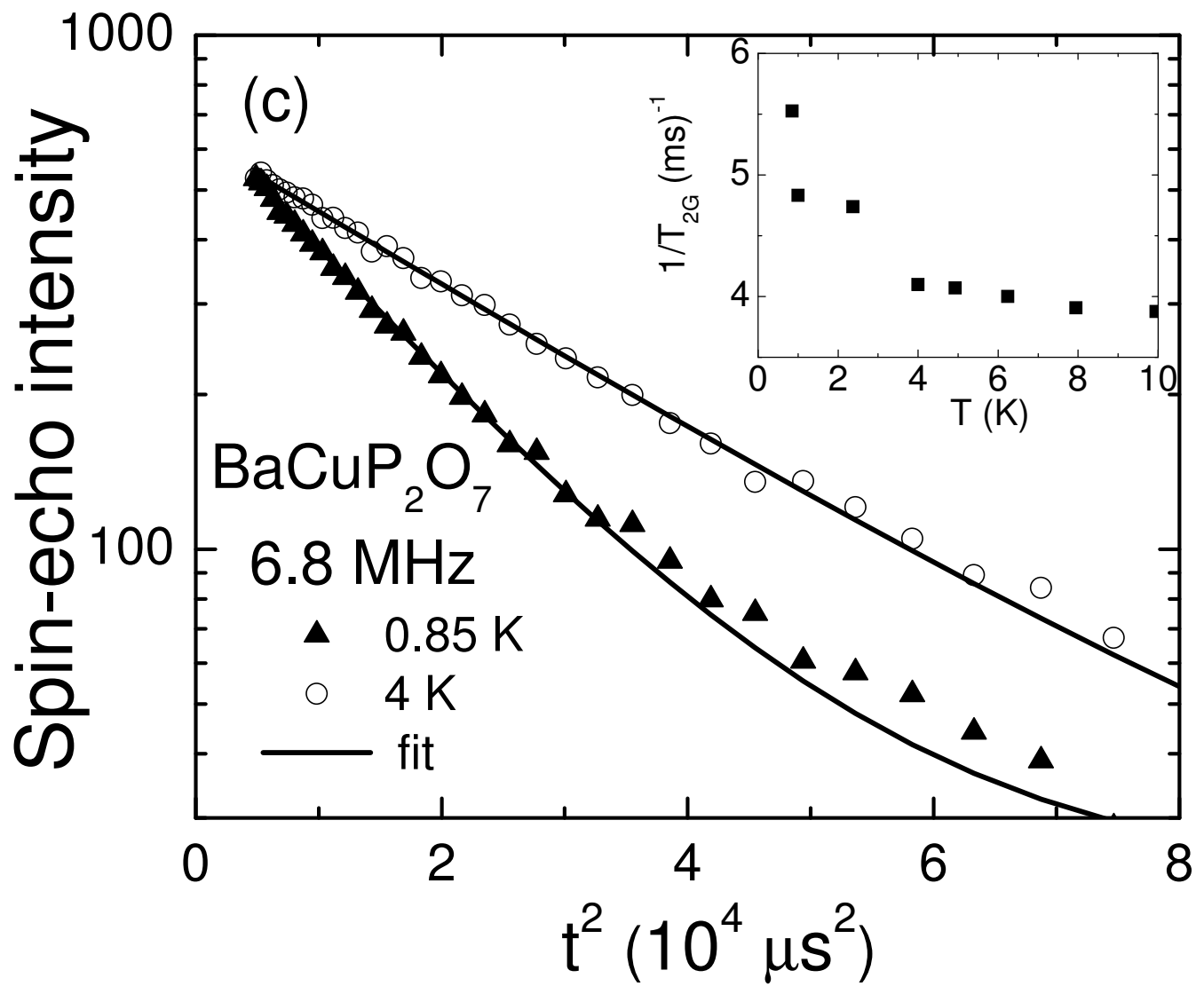


Fig. 8 (c), R. Nath et al.

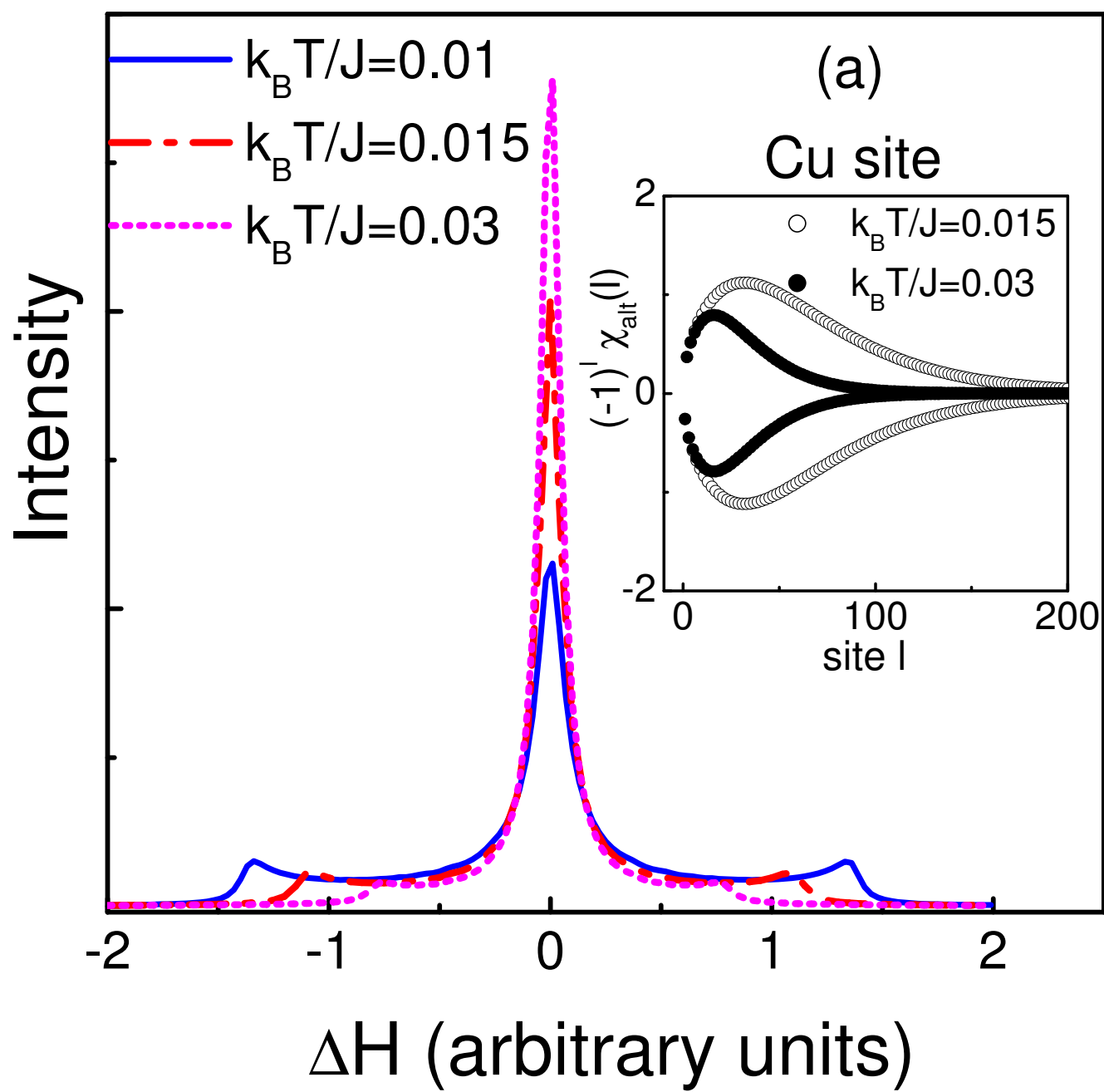


Fig. 9 (a), R. Nath et al.

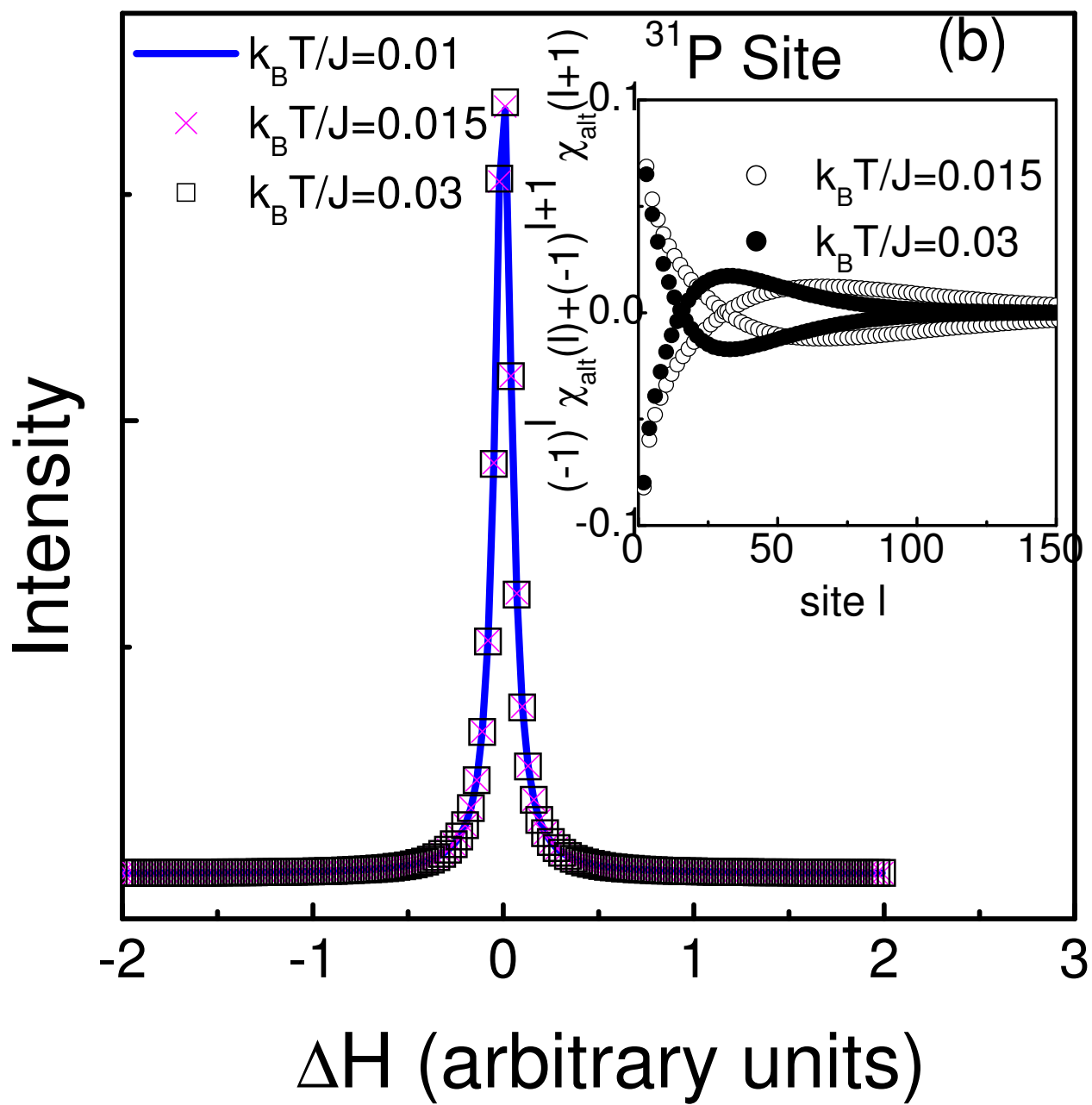


Fig. 9 (b), R. Nath et al.

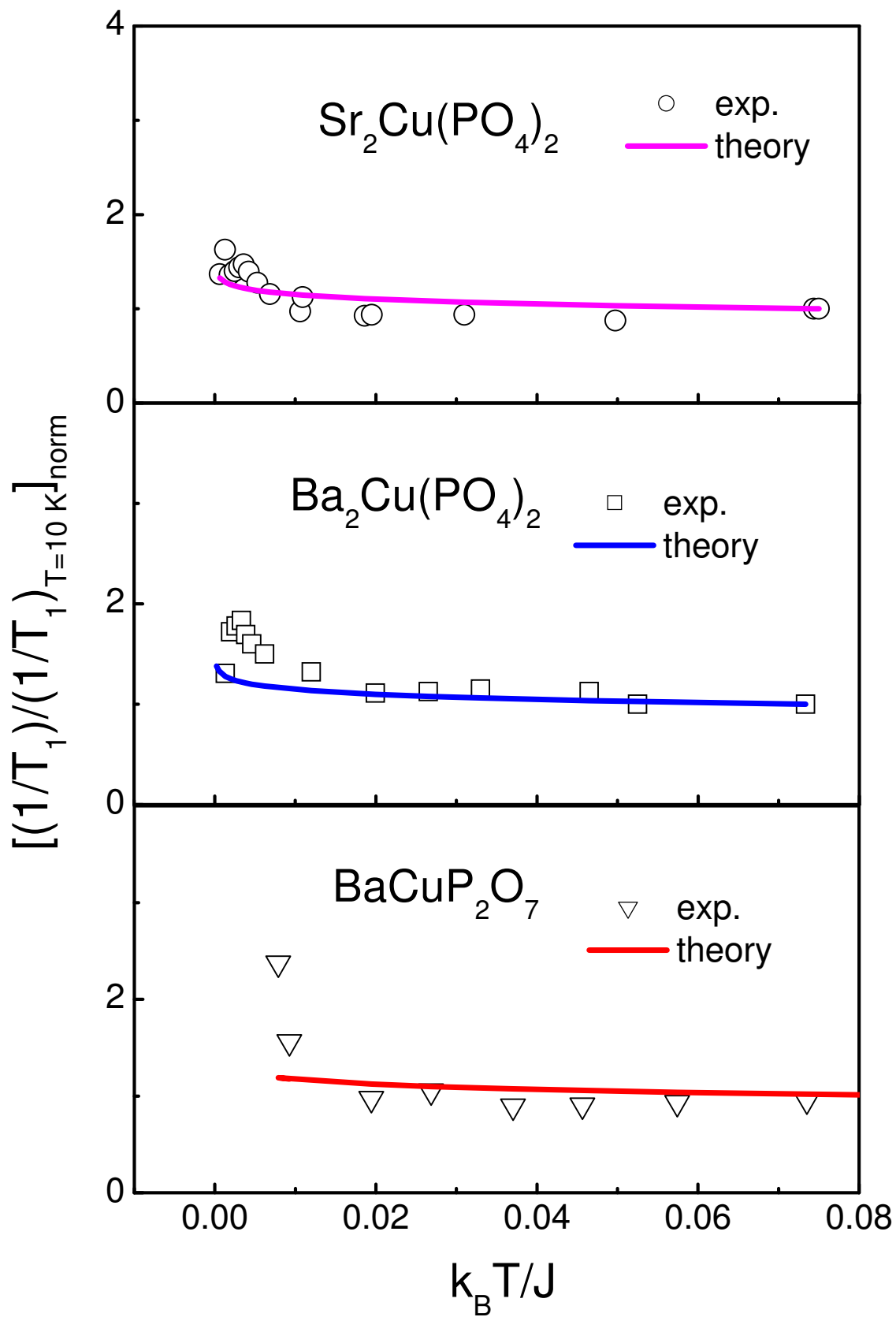


Fig. 10, R. Nath et al.